STAMBPL1 activates the GRHL3/HIF1A/VEGFA axis through interaction with FOXO1 to promote angiogenesis in triple-negative breast cancer

Huan Fang[1,2#], Huichun Liang[1#], Chuanyu Yang[1], Dewei Jiang[1], Qianmei Luo[1], Wenming Cao[3*], Huifeng Zhang[4*], Ceshi Chen[5,6,1*]

1. Kunming Institute of Zoology, Chinese Academy of Sciences, Kunming, Yunnan, China.

2. Kunming College of Life Sciences, University of Chinese Academy of Sciences, Kunming, Yunnan, China.

3. The Department of Breast Medical Oncology, Zhejiang Cancer Hospital, Hangzhou 310022, China.

4. Department of Pharmacy, the First People's Hospital of Yunnan Province/the Affiliated Hospital of Kunming University of Science and Technology, Kunming, Yunnan Province, China

5. Academy of Biomedical Engineering, Kunming Medical University, Kunming 650500, China.

6. The Third Affiliated Hospital, Kunming Medical University, Kunming 650118, China.

# These authors contributed equally to this work.

* Corresponding authors: Wenming Cao, E-mail: caowm@zjcc.org.cn; Huifeng Zhang, E-mail: zhanghuifeng92@163.com; or Ceshi Chen, E-mail: chenc@kmmu.edu.cn.

Abstract

In the clinic, anti-tumor angiogenesis is commonly employed for treating recurrent, metastatic, drug-resistant triple-negative and advanced breast cancer. Our previous research revealed that the deubiquitinase STAMBPL1 enhances the stability of MKP-1, thereby promoting cisplatin resistance in breast cancer. In this study, we discovered that STAMBPL1 could upregulate the expression of the hypoxia-inducible factor HIF1α in breast cancer cells. Therefore, we investigated whether STAMBPL1 promotes tumor angiogenesis. We demonstrated that STAMBPL1 increased *HIF1A* transcription in a non-enzymatic manner, thereby activating the HIF1α/VEGFA signaling pathway to facilitate TNBC angiogenesis. Through RNA-seq analysis, we identified the transcription factor GRHL3 as a downstream target of STAMBPL1 that is responsible for mediating *HIF1A* transcription. Furthermore, we discovered that STAMBPL1 regulates *GRHL3* transcription by interacting with the transcription factor FOXO1. These findings shed light on the role and mechanism of STAMBPL1 in the pathogenesis of breast cancer, offering novel targets and avenues for the treatment of triple-negative and advanced breast cancer.

Keywords Triple-negative breast cancer, tumor angiogenesis, transcription regulation

Introduction

Triple-negative breast cancer (TNBC) is a subtype of breast cancer characterized by a lack of expression of estrogen receptor (ER), progesterone receptor (PR), and human epidermal growth factor receptor 2 (HER2). Despite representing only 10–15% of all breast cancer cases, it is associated with a greater risk of recurrence, metastasis, and resistance to chemotherapy, leading to a poorer prognosis than other types of breast cancer[1]. Therefore, understanding the pathogenesis of this subtype of breast cancer and identifying effective treatment targets are key areas of research focus and challenge. In the clinic, in addition to surgery, radiotherapy, and chemotherapy, treatment approaches for TNBC also include the use of epidermal growth factor receptor (EGFR) inhibitors, poly (ADP-ribose) polymerase (PARP) inhibitors, immune checkpoint inhibitors, and anti-angiogenic therapies[2, 3].

For solid tumors, the survival, proliferation, and invasion of cancer cells rely on surrounding blood vessels to provide nutrients and oxygen. Cancer cells can increase the synthesis and secretion of the vascular endothelial growth factor A (VEGFA), activate endothelial cells in neighboring blood vessels through paracrine pathways, and stimulate tumor angiogenesis[4]. Therefore, investigating the upstream molecular mechanisms that activate VEGFA in cancer cells offers new targets for inhibiting TNBC angiogenesis via disruption of this signaling pathway.

The deubiquitinase STAMBPL1 (also known as AMSH-LP) belongs to the AMSH family and cleaves K63-linked polyubiquitin chains[5]. STAMBPL1 stabilizes XIAP to inhibit apoptosis in prostate cancer cells[6] and confers resistance to honokiol-induced apoptosis in various cancer cell types by stabilizing Survivin and c-FLIP[7]. Our previous research demonstrated that STAMBPL1 enhances cisplatin resistance in TNBC cells through the stabilization of MKP-1[8].

In this study, we discovered that, independent of its deubiquitinating enzyme activity, STAMBPL1 upregulates HIF1α expression in TNBC cells. We aimed to investigate the molecular mechanism by which it upregulates HIF1α and explore its role in tumor angiogenesis in TNBC.

FOXO1, a member of the forkhead box transcription factor family, regulates various physiological and pathological processes, such as cell proliferation, apoptosis, autophagy, and oxidative stress[9]. In breast cancer, FOXO1 enhances the stemness of cancer cells by promoting *SOX2* transcription[10] and confers resistance to chemotherapy drugs in basal-like breast cancer cells by activating *KLF5* transcription[11]. Furthermore, FOXO1 plays a crucial role in angiogenesis by upregulating VEGFA transcription[12]. However, the specific mechanism by which FOXO1 regulates VEGFA transcription remains unclear, and its role in tumor angiogenesis in TNBC requires further investigation.

In this study, we discovered that STAMBPL1 facilitates the transcriptional regulation of *GRHL3* by interacting with FOXO1, consequently enhancing *HIF1A* transcription through GRHL3 to activate the HIF1α/VEGFA pathway. This results in increased endothelial cell activity via paracrine signaling, thereby promoting tumor angiogenesis in TNBC.

Methods

Cell lines and reagents

All cell lines used in this study, including HCC1806, HCC1937, and HEK293T cells, were purchased from ATCC (American Type Culture Collection, Manassas, VA, USA) and validated by short tandem repeat (STR) analysis, and these cell lines tested negative for mycoplasma contamination. HCC1806 and HCC1937 cells were cultured in RPMI 1640 medium supplemented with 5% FBS. HEK293T cells were cultured in DMEM (Thermo Fisher, Grand Island, USA) with 5% FBS at 37°C with 5% CO_2. Primary human umbilical vein endothelial cells (HUVECs) were maintained in an EGM-2 Bullet Kit (CC-3162, Lonza, USA). AS1842856 (Cat#HY-100596) and apatinib (Cat#HY-13342S) were purchased from MCE (New Jersey, USA).

Plasmid construction and stable STAMBPL1, GRHL3 and FOXO1 overexpression

We constructed the full-length *STAMBPL1/GRHL3/FOXO1* genes and then subcloned them into the pCDH lentiviral vector. The packaging plasmids (pMDLg/pRRE, pRSV-Rev, and pCMV-VSV-G) and the pCDH-STAMBPL1/GRHL3/FOXO1 expression plasmid were cotransfected into HEK293T cells (2×10^6 in 10 cm plates) to produce lentiviruses. Following transfection for 48 hours, the lentivirus was collected and used to infect HCC1806 and HCC1937 cells. Forty-eight hours later, puromycin (2 μg/ml) was used to screen the cell populations.

Stable knockdown of STAMBPL1 and GRHL3

The pSIH1-H1-puro shRNA vector was used to express STAMBPL1, GRHL3 and luciferase (LUC) shRNAs. *STAMBPL1* shRNA#1, 5'-GGAGCATCAGAGATTGATA-3'; *STAMBPL1* shRNA#2, 5'-GCTGCTATGCCTGACCATA-3'; *GRHL3* shRNA#1, 5'-

96 CCTTGAGCTTCCTCTATGA-3'; *GRHL3* shRNA#2, 5'-AGAGGAAGATGCGCGATGA-3';
97 *Luciferase* shRNA, 5'-CUUACGCUGAGUACUUCGA-3'; HCC1806 and HCC1937 cells were
98 infected with lentivirus. Stable populations were selected via the use of 1 to 2 mg/mL puromycin.
99 The knockdown effect was evaluated by Western blotting.

100 **RNA interference**

101 The siRNA target sequences used in this study were as follows: *STAMBPL1* siRNA#1, 5'-
102 GGAGCATCAGAGATTGATA-3'; *STAMBPL1* siRNA#2, 5'-GCTGCTATGCCTGACCATA-3';
103 *GRHL3* siRNA#1, 5'-CCTTGAGCTTCCTCTATGA-3'; *GRHL3* siRNA#2, 5'-
104 AGAGGAAGATGCGCGATGA-3'; *HIF1α* siRNA#1, 5'-AAGAGGTGGATATGTCTGG-3'; *HIF1α*
105 siRNA#2, 5'-CGTCGAAAAGAAAAGTCTCTT-3'; *FOXO1* siRNA#1, 5'-
106 CCCAGAUGCCUAUACAAAC-3'; and *FOXO1* siRNA#2, 5'-CTCAAATGCTAGTACTATTAG-3'.
107 All siRNAs were synthesized by RiboBio (RiboBio, China) and transfected at a final
108 concentration of 50 nM.

109 **Western blotting (WB) and antibodies**

110 The WB procedure was described in our previous study[13]. Anti-STAMBPL1 (sc-376526) and
111 anti-GAPDH (sc-25778) antibodies were purchased from Santa Cruz Biotechnology (Santa
112 Cruz, CA, USA). Anti-FOXO1 (#2880S) and anti-HIF1α (#36169S) antibodies were purchased
113 from CST. Anti-β-actin (A5441) and anti-GST (G7781) antibodies were purchased from Sigma–
114 Aldrich (St. Louis, MO, USA). The anti-Flag (ab205606) antibody was purchased from Abcam.

115 **Real-time polymerase chain reaction (RT–qPCR)**

116 Total RNA was extracted via TRIzol (Invitrogen, 15596026). One microgram of total RNA was
117 reverse transcribed to cDNA according to the manufacturer's instructions for the HiScript II QRT

118 SuperMix for qPCR Kit (Vazyme, R223-01). For quantitative PCR (RT–qPCR), the SYBR Green
119 Select Master Mix system (Applied Biosystems, 4472908, USA) was used on an ABI-7900HT
120 system (Applied Biosystems, 4351405). The primers used for PCR were as follows: 18S
121 forward, 5′-CTCAACACGGGAAACCTCAC-3′; 18S reverse, 5′-
122 CGCTCCACCAACTAAGAACG-3′; HIF1α forward, 5′-AAGTCTGCAACATGGAAGGTAT-3′;
123 HIF1α reverse, 5′-TGAGGAATGGGTTCACAAATC-3′; VEGFA forward, 5′-
124 TGAGGAATGGGTTCACAAATC-3′; VEGFA reverse, 5′-ATCTGCATGGTGATGTTGGA-3′;
125 GLUT1 forward, 5′-TCGTCGGCATCCTCATCGCC-3′; GLUT1 reverse, 5′-
126 CCGGTTCTCCTCGTTGCGGT-3′; GRHL3 forward, 5′-GGGGCTGAGGAATGCGATCT-3′; and
127 GRHL3 reverse, 5′-AATTTTGCCGTCCAGCTCCC-3′.

128 **Cell proliferation and migration assays**

129 To detect the proliferation of HUVECs, we used the Click-iT™ EdU Alexa Fluor™ 647 Imaging
130 Kit (Invitrogen) according to the manufacturer's protocol. Briefly, HUVECs were seeded on
131 coverslips (BD Biosciences) at 0.5×10^5 cells per well. The next day, the supernatants were
132 discarded, and the cells were cultured with conditioned medium (CM). Six hours later, the cells
133 were incubated with EdU in CM for 4 hours, followed by fixation and staining. For each sample,
134 three random fields were observed via fluorescence microscopy, and the total numbers of cells
135 and EdU-positive cells were counted. To detect the migration of HUVECs, we performed a
136 wound-healing assay. Twenty-four hours after seeding, the supernatants of the HUVECs were
137 discarded, and the cells were scratched and cultured with CM for 24 hours. Wound closure was
138 imaged via microscopy. For each image, the gap width was analyzed via ImageJ.

139 **Tube formation assays**

140 HUVECs (1 × 10^4) in CM were seeded onto Matrigel (BD Biosciences)-coated μ-Slide
141 angiogenesis plates (ibidiGmbH, Munich, Germany). At 6 hours after seeding, images were
142 taken via microscopy and then analyzed with ImageJ. The total branch length was measured.

143 **Chromatin immunoprecipitation assays**

144 After the sample preparation was completed, the subsequent experimental steps were
145 performed according to the instructions of the Simple ChIP (R) Plus Kit (CST, # 9005). The PCR
146 primers for amplifying the region of interest on the HIF1α gene promoter were as follows: 5′-
147 GACTGACAGGCTTGAAGTTTATGC-3′ and 5′-TGTTGCTGTAAACTTCAAGGGAAA-3′, and
148 the PCR primers for amplifying the region of interest on the GRHL3 gene promoter were as
149 follows: 5′-TTCTATCCCTTCTGTGCTGACCA-3′ and 5′-TGTGCCAGACCCTACTCTGGG-3′.

150 **Dual-luciferase reporter assays**

151 The DNA fragments HIF1α and GRHL3 were amplified from MCF10A cell genomic DNA via
152 PCR template and then cloned and inserted into the pGL3-Basic vector. HEK293T cells were
153 seeded in 24-well plates and transfected with pCDH-GRHL3-3×Flag or pCDH-FOXO1-3×Flag
154 and pGL3 luciferase reporter plasmids (both 600 ng/well) together with the pCMV-Renilla
155 control (5 ng/well). After transfection for 48 h, the cell lysates were collected, and the luciferase
156 activities were detected via the dual-luciferase reporter assay system (Promega, USA). For the
157 WT HIF1α promoter (with the GRHL3 binding motif), the primers used for PCR were as follows:
158 forward, 5′-gctagcccgggctcgagatctCCACTGCGCTCCAGCCTG-3′; reverse, 5′-
159 cagtaccggaatgccaagcttCCTCAGACGAGGCAGCACTG-3′. For the mutant HIF1α promoter
160 (without the GRHL3 binding motif), the primers used for PCR were as follows: forward, 5′-
161 TCTTTCCCTGAGGCCTTCCTATATGCTTAT-3′; reverse, 5′-

162 ATAAGCATATAGGAAGGCCTCAGGGAAAGA-3′. For the WT GRHL3 promoter (with the
163 FOXO1 binding motif), the primers used for PCR were as follows: forward, 5′-
164 gctagcccgggctcgagatctATTAACAAGGGTGACTGAAGAGGG-3′; reverse, 5′-
165 cagtaccggaatgccaagcttTGGAGGTATACCTCAACAGGTGC-3′. For the mutant GRHL3
166 promoter (without the FOXO1 binding motif), the primers used for PCR were as follows: forward,
167 5′-CTCCCCCACCAAACAAAGAAGGAGAACACCCC-3′; reverse, 5′-
168 GGGGTGTTCTCCTTCTTTGTTTGGTGGGGGAG-3′.

169 **Immunofluorescence staining**

170 HEK293T cells plated on cell culture slides were transfected with the STAMBPL1 and FOXO1
171 expression plasmids. Two days after transfection, the cells were fixed in 3.7%
172 polyformaldehyde at 4°C overnight. After being blocked with 5% BSA at room temperature for
173 1 hour, the cells were stained with anti-STAMBPL1 (mouse) and anti-FOXO1 (rabbit) antibodies
174 at 4°C overnight. The cells were subsequently stained with both an Alexa Fluor647-labeled anti-
175 mouse secondary antibody and a FITC-labeled anti-rabbit secondary antibody (ZSGB-Bio,
176 Beijing, China) at room temperature for 1 hour. Nuclei were stained with DAPI (Biosharp,
177 BL739A) for 15 min. Images were captured via a confocal microscope.

178 **Immunoprecipitation and GST pull-down**

179 For endogenous protein interaction, cell lysates were first incubated with anti-FOXO1
180 antibodies or rabbit IgG (2729S; Cell Signaling Technology) and then incubated with protein
181 A/G magnetic beads (HY-K0202; MCE). For the GST pull-down assay, the cell lysates were
182 directly incubated with Glutathione Sepharose 4B (10312185; Cytiva) overnight at 4°C. For the
183 IP-Flag assay, cell lysates were directly incubated with anti-Flag magnetic beads (HY-K0207;

184 MCE) overnight at 4°C. The precipitates were washed four times with 1 ml of lysis buffer, boiled
185 for 10 minutes with 1×SDS sample buffer, and subjected to WB analysis.

186 **Xenograft experiments**

187 We purchased 5- to 6-week-old female BALB/c nude mice from SLACCAS (Changsha, China).
188 Animal feeding and experiments were approved by the animal ethics committee of Kunming
189 Institute of Zoology, Chinese Academy of Sciences. HCC1806-shLuc, HCC1806-shSTAMBPL1,
190 or HCC1806-shGRHL3 cells and HCC1806-PCDH-Vector or HCC1806-PCDH-STAMBPL1
191 cells (1×10^6 in Matrigel (BD Biosciences, NY, USA)) were implanted into the mammary fat
192 pads of the mice. When the tumor volume reached approximately 50 mm^3, the nude mice were
193 randomly assigned to the control or treatment groups (n = 4/group). The control group was
194 given vehicle alone, and the treatment group received the FOXO1 inhibitor AS1842856 (10
195 mg/kg), the VEGFR inhibitor apatinib (50 mg/kg), and the FOXO1 inhibitor AS1842856
196 combined with the VEGFR inhibitor apatinib via intragastric administration every two days for
197 20 days. The tumor volume was calculated as follows: tumor volume was calculated by the
198 formula ($\pi \times \text{length} \times \text{width}^2$)/6. The maximal tumor size permitted by the animal ethics
199 committee of Kunming Institute of Zoology, Chinese Academy of Sciences, and the maximal
200 tumor size in this study was not exceeded.

201 **Immunohistochemical staining**

202 The xenograft tumor tissues were fixed in 3.7% formalin solution. The immunohistochemistry
203 was performed on 4-μm-thick paraffin sections after pressure-cooking for antigen retrieval. An
204 anti-CD31 primary antibody (1:400, Abcam, ab28364) was used. After 12 h, the slides were
205 washed three times with PBS and incubated with secondary antibodies (hypersensitive

enzyme-labeled goat anti-mouse/rabbit IgG polymer (OriGene, China) at room temperature for 20 min, DAB concentrated chromogenic solution (1:200 dilution of concentrated DAB chromogenic solution)), counterstained with 0.5% hematoxylin, dehydrated with graded concentrations of ethanol for 3 min each (70%–80%–90%–100%), and finally stained with dimethyl benzene. The immunostained slides were evaluated via light microscopy, and the number of microvessels with positive CD31 expression was counted.

Statistical analysis

All the graphs were created via GraphPad Prism software version 8.0. Comparisons between two independent groups were assessed via two-tailed Student's *t* tests. One-way analysis of variance with least significant differences was used for multiple group comparisons. *P* values of < 0.05, 0.01 or 0.001 were considered to indicate statistically significant results, and comparisons that were significant at the 0.05 level are indicated by *, those at the 0.01 level are indicated by **, and those at the 0.001 level are indicated by ***.

Results

STAMBPL1 upregulates HIF1α in a non-enzymatic manner in TNBC cells.

Our previous research revealed that STAMBPL1, a deubiquitinase, promotes cisplatin resistance in TNBC by stabilizing MKP1[8]. To further investigate the role and mechanism of STAMBPL1 in TNBC, we discovered that the knockdown of STAMBPL1 can inhibit hypoxia-induced HIF1α expression (Fig.1A) and suppress the transcription of the HIF1α downstream genes *VEGFA* and *GLUT1* (Fig.1B-E). Under normoxic conditions, both STAMBPL1 and its enzymatically mutated variant (E292A) can upregulate the protein expression of HIF1α (Fig.1F). These findings suggest that STAMBPL1 enhances the expression of HIF1α in breast cancer cells through a non-DUB enzyme activity mechanism.

STAMBPL1 promotes *HIF1A* transcription and activates the HIF1α/VEGFA axis.

To elucidate how STAMBPL1 upregulates HIF1α, we examined the transcription levels of *HIF1A* when STAMBPL1 was knocking down under hypoxia. These results indicate that knocking down STAMBPL1 significantly inhibits the transcription of *HIF1A* (Fig.2A-C). At the same time, we detected the transcription level of HIF1A and VEGFA when STAMBPL1 was overexpressing under normoxia. Data showed that STAMBPL1 overexpression increased the transcription of *HIF1A* (Fig.4E and Fig. S3E) and *VEGFA* (Fig.2E and 2G). The ability of STAMBPL1 to induce *VEGFA* transcription was blocked by HIF1α knockdown (Fig.2D-G). These findings suggested that STAMBPL1 activated the HIF1α/VEGFA axis through enhancing the transcription of *HIF1α*.

STAMBPL1 in TNBC cells enhances the activity of HUVECs and promotes TNBC angiogenesis.

241 The conditioned medium (CM) from TNBC cells with STAMBPL1 knockdown inhibited the
242 proliferation (Fig.3A-B, and Fig.S1A-B), migration (Fig.3C-D, and Fig.S1C-D), and tube
243 formation (Fig.3E-F, and Fig.S1E-F) of HUVECs. When STAMBPL1 was overexpressed in
244 TNBC cells, the conditioned medium of HCC1806 and HCC1937 cells promoted the ability of
245 HUVECs to proliferate (Fig.S2A and Fig.S2D), migrate (Fig.S2B and Fig.S2E), and form tubes
246 (Fig.S2C and Fig.S2F), which could be reversed by knocking down HIF1α in TNBC cells. These
247 findings suggest that STAMBPL1 activates the HIF1α/VEGFA axis in TNBC cells, leading to
248 enhanced abilities of HUVECs through a paracrine pathway. Knocking down STAMBPL1
249 inhibited the growth of HCC1806 xenografts in mice (Fig.3G-I) and decreased the number of
250 microvessel in tumor tissue (Fig.3J-K), indicating that STAMBPL1 promoted tumor
251 angiogenesis.

252 **STAMBPL1 promotes *HIF1A* transcription via the upregulation of GRHL3.**

253 By silencing the *STAMBPL1* gene in HCC1806 cells subjected to 10 hours of hypoxia, we
254 performed RNA-seq analysis to investigate the mechanism by which STAMBPL1 promotes
255 *HIF1A* transcription. We found that silencing of STAMBPL1 resulted in the downregulation of
256 27 genes (of which only 18 were annotated). Of these 18 genes, except for GRHL3, which is a
257 transcription factor reported to be involved in gene transcription regulation, the remaining 17
258 genes have no documented association with RNA transcription, stability, or modification (Fig.4A
259 and Fig.S3A). Silencing of STAMBPL1 inhibited *GRHL3* transcription in both HCC1806 and
260 HCC1937 cells (Fig.4B and Fig.S3B). Conversely, the overexpression of STAMBPL1 promoted
261 *GRHL3* transcription (Fig.4D and Fig.S3D). Furthermore, the stimulatory effects of STAMBPL1
262 on the HIF1α/VEGFA axis (Fig. 4C-F and Fig.S3C-F) and on HUVECs (Fig.4G-I and Fig.S3G-

263 I) were reversed by GRHL3 knockdown. These findings suggest that STAMBPL1 activates the
264 HIF1α/VEGFA axis by upregulating GRHL3.

265 **GRHL3 enhances *HIF1A* transcription by binding to its promoter.**

266 On the basis of the GRHL binding motif (Fig.5A), a GRHL binding sequence was identified in
267 the *HIF1A* promoter (Fig.5B). ChIP and luciferase assays revealed that GRHL3 bound to the
268 *HIF1A* promoter (Fig.5D) and increased its activity (Fig.5E). Knockdown of GRHL3 (Fig.5G and
269 Fig.S4B) resulted in decreased expression of HIF1α at both the mRNA (Fig.5H and Fig.S4C)
270 and protein levels (Fig.5F and Fig.S4A), leading to suppressed *VEGFA* transcription (Fig.5I and
271 Fig.S4D), indicating that GRHL3 promotes *HIF1A* transcription by binding to its promoter.
272 Furthermore, conditioned medium from TNBC cells with GRHL3 knockdown inhibited HUVEC
273 proliferation, migration, and tube formation (Fig.5J-L and Fig.S4E-G). The overexpression of
274 GRHL3 in TNBC cells activated the HIF1α/VEGFA axis (Fig.6A-B and Fig.S4H-J), resulting in
275 increased proliferation, migration, and tube formation in HUVECs. This effect was reversed by
276 knocking down HIF1α in TNBC cells (Fig.6C-E and Fig.S4K-M). Knockdown of GRHL3 (Fig.6F)
277 also inhibited tumor growth in HCC1806 xenograft mice (Fig.6G-I) and reduced the number of
278 microvessel in tumor tissues (Fig.6J-K).

279 **STAMBPL1 mediates *GRHL3* transcription by interacting with FOXO1.**

280 Our previous study demonstrated that STAMBPL1 is localized in the nucleus[8]. This protein
281 may promote the transcription of GRHL3 through interactions with other transcription factors.
282 Previous studies have indicated that FOXO1 acts as an upstream transcription factor of
283 GRHL3[14]. Therefore, we aimed to investigate whether STAMBPL1 promotes GRHL3
284 transcription via FOXO1. Our experimental data revealed that knockdown of FOXO1 in TNBC

285 cells not only inhibited the GRHL3/HIF1α/VEGFA axis (Fig.7A-D and Fig.S5A-D) but also
286 reversed the stimulatory effects of STAMBPL1 on this axis (Fig.7E-H). Furthermore, FOXO1
287 was found to bind to the promoter region of GRHL3 (Fig.7I and Fig.S5F) and enhance its
288 transcriptional activity (Fig.7J). STAMBPL1 was shown to increase the transcriptional activation
289 of FOXO1 at the GRHL3 promoter (Fig.7K), and it also bound to the GRHL3 promoter which
290 could be disrupted by FOXO1 knockdown (Fig.7L). However, the overexpression of STAMBPL1
291 and its enzymatic activity mutants did not affect the protein expression level of FOXO1
292 (Fig.S5E). To investigate the mechanism by which STAMBPL1 promotes GRHL3 transcription
293 through FOXO1, we conducted immunofluorescence and immunoprecipitation assays. We
294 observed the colocalization of STAMBPL1 and FOXO1 in the nucleus (Fig.7M) and identified
295 an interaction between them in HCC1937 cells (Fig.7N). Through the generation of a series of
296 Flag-FOXO1/GST-fused STAMBPL1 deletion mutants, we mapped the regions of the proteins
297 responsible for this interaction (Fig.S5G–H). The results of the GST pulldown assay indicated
298 that the N-terminus (1–140 aa) of STAMBPL1 interacted with FOXO1 (Fig.S5I). Additionally, an
299 immunoprecipitation assay revealed an interaction between the FOXO1 protein (250–596 aa)
300 and STAMBPL1 (Fig.S5J). These findings suggest that STAMBPL1 promotes GRHL3
301 transcription by interacting with FOXO1.

302 **The combination of VEGFR and FOXO1 inhibitors synergistically suppresses TNBC**
303 **xenograft growth.**

304 Through an analysis of the Metabric database in BCIP (http://www.omicsnet.org/bcancer), it
305 was observed that while the expression levels of STAMBPL1, FOXO1, and GRHL3 in breast
306 cancer tissues are not universally elevated compared to adjacent non-cancerous tissues, but

307 their expression levels in TNBC are significantly higher than those in non-TNBC (Fig.8A-C and
308 Fig.S6A-C). To assess the potential therapeutic efficacy of cotreatment with the FOXO1
309 inhibitor AS1842856 and the VEGFR inhibitor apatinib *in vivo*, we conducted animal
310 experiments in nude mice. HCC1806 cells overexpressing STAMBPL1 were orthotopically
311 implanted into the mammary fat pads of 6-week-old female mice (n=16/group). Once the tumor
312 volume reached approximately 50 mm^3, the mice were divided into four subgroups to receive
313 apatinib (50 mg/kg, once every two days), AS1842856 (10 mg/kg, once every two days), a
314 combination of both drugs, or vehicle control for 20 days. Our findings indicated that STAMBPL1
315 overexpression enhanced breast cancer cell growth *in vivo*. While the individual inhibitory
316 effects of the FOXO1 and VEGFR inhibitors on tumor growth were not significant, the combined
317 treatment markedly suppressed tumor growth in nude mice (Fig.8E-G). Importantly, the drug
318 treatments did not affect the body weights of the mice (Fig.8H). These results suggest that the
319 combined administration of AS1842856 and apatinib effectively inhibits tumor growth in nude
320 mice.
321

Discussion

In this study, we discovered that STAMBPL1 promotes angiogenesis in TNBC by activating the HIF1α/VEGFA pathway independently of its enzymatic activity. Through RNA-seq analysis, we revealed that STAMBPL1 positively regulates the transcription of *GRHL3*. Furthermore, we demonstrated that GRHL3 binds to the promoter of the *HIF1A* gene, thereby increasing its transcription. Additionally, we found that STAMBPL1 interacts with FOXO1 to facilitate the transcription of GRHL3/HIF1α/VEGFA. Importantly, we confirmed that the combination of the FOXO1 inhibitor AS1842856 and the VEGFR inhibitor apatinib effectively inhibited tumor growth in nude mice. These findings suggest that both STAMBPL1 and FOXO1 may be potential therapeutic targets for inhibiting angiogenesis in TNBC. This study is the first to uncover the role of STAMBPL1 in promoting angiogenesis through the FOXO1/GRHL3/HIF1α axis. Furthermore, a novel transcription factor, GRHL3, which regulates the transcription of HIF1α was identified. These findings provide valuable insights for developing new therapeutic strategies to target TNBC.

The role of STAMBPL1 in tumors has not been fully recognized. Recent studies have reported its involvement in the epithelial–mesenchymal transition of various cancers, and its absence has been shown to affect the mesenchymal phenotype of lung and breast cancer[15]. Our previous research demonstrated that STAMBPL1 can stabilize MKP1 through deubiquitination and that the deletion of STAMBPL1 and MKP1 increases the sensitivity of breast cancer cells to cisplatin[16], suggesting that STAMBPL1 may be a potential therapeutic target for breast cancer. However, the mechanism by which STAMBPL1 activates the transcriptional activity of FOXO1 has not been elucidated. The transcriptional activity of FOXO1 is primarily regulated

344 by its nucleocytoplasmic shuttling process[17]. The PI3K/AKT pathway promotes the
345 phosphorylation of FOXO1, resulting in the formation of a complex with members of the 14-3-
346 3 family (including 14-3-3σ, 14-3-3ε, and 14-3-3ζ), which facilitates its export from the nucleus
347 and inhibits its transcriptional activity[18, 19]. It's reported that TDAG51 prevents the binding of
348 14-3-3ζ to FOXO1 in the nucleus by interacting with FOXO1, thereby enhancing its
349 transcriptional activity through increased accumulation within the nucleus[20]. Our results
350 indicate that the overexpression of STAMBPL1 and STAMBPL1-E292A did not affect the protein
351 levels of FOXO1 (Fig.7E and Fig.S5E), but STAMBPL1 co-localizes with FOXO1 in the nucleus
352 (Fig.7M) and interacts with it (Fig.7N and Fig.S5I-J). This suggests that STAMBPL1 enhances
353 the transcriptional activity of FOXO1 on GRHL3 by interacting with nuclear FOXO1. So, it will
354 be important to develop a *Stambpl1* knockout mouse model to investigate the exact role of
355 STAMBPL1 in TNBC. Additionally, we need to develop HIF1α and FOXO1 antibodies suitable
356 for immunohistochemistry to detect their expression in TNBC clinical samples.

357 Several studies have reported that FOXO1 inhibits tumor angiogenesis[21-25]. Studies have
358 shown that M2 macrophage-derived exosomal miR-942 promotes the migration and invasion
359 of lung adenocarcinoma cells and facilitates angiogenesis by binding to FOXO1 to alleviate the
360 inhibition of β-catenin, in which the upregulation of FOXO1 induces a decrease in cell invasion
361 and angiogenesis *in vitro*[21]. FOXO1 inhibits gastric cancer growth and angiogenesis under
362 hypoxic conditions via inactivation of the HIF1α-VEGF pathway, possibly in association with
363 SIRT1[22]. Cancer-associated fibroblast (CAF)-derived extracellular vesicles (EVs) deliver
364 miR-135b-5p into colorectal adenocarcinoma cells to downregulate FOXO1 and promote
365 HUVEC proliferation, migration, and angiogenesis[23]. Colorectal cancer cell-derived

exosomes overexpressing miR-183-5p promote the proliferation, migration and tube formation of HMEC-1 (human microvascular endothelial cells) cells through the inhibition of FOXO1[24]. Bladder cancer cell-derived exosomal miR-1247-3p facilitates angiogenesis by inhibiting FOXO1 expression[25]. However, the role of FOXO1 in breast cancer angiogenesis has not been studied, and our study revealed that FOXO1 can promote the expression of HIF1α and VEGFA, suggesting that it may play a role in promoting angiogenesis in breast cancer.

Studies have demonstrated that the AKT-FOXO1 signaling pathway regulates the expression of GRHL3. To investigate this, the researchers utilized a previously published ChIP-seq dataset for FOXO1 from human endometrial stromal cells. They reported that FOXO1 occupied BRD4-bound enhancers near the *GRHL3* gene. The authors subsequently confirmed that the removal of EGF and insulin from the growth medium significantly increased the expression of GRHL3, but the administration of the FOXO1 inhibitor AS1842856 partially blocked the induced expression of GRHL3[14]. These results suggest that FOXO1 plays a regulatory role upstream of GRHL3, and our study also confirmed that FOXO1 promotes the transcription of *GRHL3* by binding to its promoter.

GRHL3 is a highly conserved epidermal-specific developmental transcription factor that has recently gained attention in the field of cancer research[26]. To date, only a few genes regulated by GRHL3 have been identified. Studies have shown that GRHL3 levels are significantly reduced in human skin and head and neck squamous cell carcinomas and suggest that GRHL3 is a key tumor suppressor pathway in squamous cell carcinomas[27]. GRHL3 was also found to be induced by TNF-α in the mammary carcinoma cell line MCF-7 and was identified as a

387 TNFα-induced endothelial cell migration factor with promigratory activity as high as that of
388 VEGF[28]. However, the specific role of GRHL3 in breast cancer is unclear. Studies have
389 confirmed that GRHL3 strongly stimulates endothelial cell migration, which is consistent with
390 an angiogenic, protumorigenic function[28]. In our study, we demonstrated that GRHL3
391 promotes TNBC angiogenesis. HIF1α, a known regulator of angiogenesis, is regulated by
392 growth factors[29, 30], cytokines[31] and mitogens[32, 33]. The EGFR/Akt pathway is a known
393 positive regulator of HIF1α, potentially through mTOR[29] or independent of it[34, 35]. While
394 the mechanisms regulating HIF1α protein expression have been extensively studied, those
395 modulating HIF1α transcriptional activity remain unclear. Our study reveals for the first time that
396 GRHL3 promotes transcriptional activity by binding to the promoter of the *HIF1α* gene.

397 In this study, we utilized two triple-negative breast cancer cell lines, HCC1806 and HCC1937,
398 along with human primary umbilical vein endothelial cells (HUVECs) and a nude mouse breast
399 orthotopic transplantation tumor model to investigate the regulatory mechanism by which
400 STAMBPL1 activates the GRHL3/HIF1α/VEGFA signaling pathway through its interaction with
401 FOXO1, thereby promoting angiogenesis in TNBC. The results of this study have certain
402 limitations regarding their applicability to human TNBC biology. Furthermore, in addition to the
403 HIF1α/VEGFA signaling pathway emphasized in this study, tumor cells can continuously
404 release or upregulate various pro-angiogenic factors, such as Angiopoietin and FGF, which
405 activate endothelial cells, pericytes (PCs), cancer-associated fibroblasts (CAFs), endothelial
406 progenitor cells (EPCs), and immune cells (ICs). This leads to capillary dilation, basement
407 membrane disruption, extracellular matrix remodeling, pericyte detachment, and endothelial
408 cell differentiation, thereby sustaining a highly active state of angiogenesis[36]. It is important

409 to collect clinical TNBC tissue samples in the future to analyze the expression of the
410 STAMBPL1/FOXO1/GRHL3/HIF1α/VEGFA signaling axis. Furthermore, patient-derived
411 organoid and xenograft models are useful to elucidate the regulatory relationship of this axis in
412 TNBC angiogenesis.

413 **Conclusions**

414 In summary, STAMBPL1 promoted TNBC angiogenesis by activating the
415 GRHL3/HIF1α/VEGFA pathway via interacting with FOXO1 in a non-enzymatic manner. These
416 findings highlight the significant role of STAMBPL1 in TNBC angiogenesis and suggest that
417 targeting the STAMBL1/FOXO1/GRHL3/HIF1α/VEGFA axis could be a potential therapeutic
418 strategy to inhibit angiogenesis in TNBC.

419

420 **List of abbreviations**

421 TNBC: triple-negative breast cancer

422 ER: estrogen receptor

423 PR: progesterone receptor

424 HER2: human epidermal growth factor receptor 2

425 EGFR: epidermal growth factor receptor

426 PARP: poly (ADP-ribose) polymerase

427 VEGFA: vascular endothelial growth factor A

428 HUVECs: primary human umbilical vein endothelial cells

429 CM: conditioned medium

430 **Supplementary information**

Supplementary Data (Supplementary Material 1) are available at eLife Online.

Acknowledgements

We sincerely thank the team members for their dedication to this study.

Authors' contributions

Ceshi Chen, Huifeng Zhang, Wenmin Cao and Huichun Liang: conceptualization; Huan Fang, Huichun Liang and Ceshi Chen: data curation; Huan Fang and Huichun Liang: formal analysis, methodology and writing-original draft with help from Chuanyu Yang, Dewei Jiang and Qianmei Luo; Ceshi Chen, Huichun Liang, Huifeng Zhang, and Wenmin Cao: funding acquisition, project administration, validation, supervision and writing-review & editing.

Funding

This work was supported by National Key Research and Development Program of China (2023YFA1800500, 2020YFA0112300), National Natural Science Foundation of China (U2102203 to CC, 82203413 to HL), Biomedical Projects of Yunnan Key Science and Technology Program (202302AA310046 to CC), Yunnan Fundamental Research Projects (202301AS070050 to CC, 202201AT070290 to HL), Yunnan Revitalization Talent Support Program (Yunling Shcolar Project to CC), Yunnan (Kunming) Academician Expert Workstation (grant No. YSZJGZZ-2020025 to CC), Kunming University of Science and Technology-The First People's Hospital of Yunnan Province Joint Major Project (No. KUST-KH2022005Z), and Center of Clinical Pharmacy of the First People's Hospital of Yunnan Province Open Project (No. 2023YJZX-YX04).

Declarations

Ethics approval and consent to participate

All experimental procedures involving animals were performed in accordance to the Animal Welfare Law of China and the Guidelines for Animal Experiment of Kunming Institute of Zoology, Chinese Academy of Sciences.

Availability of data and materials

The datasets used and/or analyzed during the current study are available from the corresponding author on reasonable request.

Competing interests

The authors declare that they have no conflicts of interest.

References

1. Geyer, F.C., et al., *The Spectrum of Triple-Negative Breast Disease: High- and Low-Grade Lesions.* Am J Pathol, 2017. 187(10): p. 2139-2151.
2. Zagami, P. and L.A. Carey, *Triple negative breast cancer: Pitfalls and progress.* NPJ Breast Cancer, 2022. 8(1): p. 95.
3. Garcia, J., et al., *Bevacizumab (Avastin(R)) in cancer treatment: A review of 15 years of clinical experience and future outlook.* Cancer Treat Rev, 2020. 86: p. 102017.
4. Detmar, M., *Tumor angiogenesis.* J Investig Dermatol Symp Proc, 2000. 5(1): p. 20-3.
5. Sato, Y., et al., *Structural basis for specific cleavage of Lys 63-linked polyubiquitin chains.* Nature, 2008. 455(7211): p. 358-62.
6. Chen, X., et al., *Targeting the deubiquitinase STAMBPL1 triggers apoptosis in prostate cancer cells by promoting XIAP degradation.* Cancer Lett, 2019. 456: p. 49-58.
7. Woo, S.M., et al., *Honokiol Enhances TRAIL-Mediated Apoptosis through STAMBPL1-Induced Survivin and c-FLIP Degradation.* Biomolecules, 2019. 9(12).
8. Liu, R., et al., *STAMBPL1 promotes breast cancer cell resistance to cisplatin partially by stabilizing MKP-1 expression.* Oncogene, 2022. 41(16): p. 2265-2274.
9. Xing, Y.Q., et al., *The regulation of FOXO1 and its role in disease progression.* Life Sci, 2018. 193: p. 124-131.
10. Yu, J.M., et al., *TRIB3 supports breast cancer stemness by suppressing FOXO1 degradation and enhancing SOX2 transcription.* Nat Commun, 2019. 10(1): p. 5720.
11. Cui, Q., et al., *DNA damage chemotherapeutic drugs suppress basal-like breast cancer growth by down-regulating the transcription of the FOXO1-KLF5 axis.* Genes Dis, 2024. 11(1): p. 91-94.
12. Jeon, H.H., et al., *FOXO1 regulates VEGFA expression and promotes angiogenesis in healing wounds.* J Pathol, 2018. 245(3): p. 258-264.
13. Chen, C., et al., *Ubiquitin-proteasome degradation of KLF5 transcription factor in cancer and untransformed epithelial cells.* Oncogene, 2005. 24(20): p. 3319-27.

14. Nagarajan, S., et al., *BRD4 promotes p63 and GRHL3 expression downstream of FOXO in mammary epithelial cells.* Nucleic Acids Res, 2017. 45(6): p. 3130-3145.
15. Ambroise, G., et al., *Systematic analysis reveals a functional role for STAMBPL1 in the epithelial-mesenchymal transition process across multiple carcinomas.* 2020. 123(7): p. 1164-1177.
16. Liu, R., et al., *STAMBPL1 promotes breast cancer cell resistance to cisplatin partially by stabilizing MKP-1 expression.* 2022. 41(16): p. 2265-2274.
17. Van Der Heide, L.P., M.F. Hoekman, and M.P. Smidt, *The ins and outs of FoxO shuttling: mechanisms of FoxO translocation and transcriptional regulation.* Biochem J, 2004. 380(Pt 2): p. 297-309.
18. Huang, H. and D.J. Tindall, *Dynamic FoxO transcription factors.* J Cell Sci, 2007. 120(Pt 15): p. 2479-87.
19. Tzivion, G., M. Dobson, and G. Ramakrishnan, *FoxO transcription factors; Regulation by AKT and 14-3-3 proteins.* Biochim Biophys Acta, 2011. 1813(11): p. 1938-45.
20. Park, E.S., et al., *TDAG51 promotes transcription factor FoxO1 activity during LPS-induced inflammatory responses.* EMBO J, 2023. 42(13): p. e111867.
21. Wei, K., et al., *M2 macrophage-derived exosomes promote lung adenocarcinoma progression by delivering miR-942.* Cancer Lett, 2022. 526: p. 205-216.
22. Kim, S.Y., et al., *Forkhead Transcription Factor FOXO1 Inhibits Angiogenesis in Gastric Cancer in Relation to SIRT1.* Cancer Res Treat, 2016. 48(1): p. 345-54.
23. Dai, X., Y. Xie, and M. Dong, *Cancer-associated fibroblasts derived extracellular vesicles promote angiogenesis of colorectal adenocarcinoma cells through miR-135b-5p/FOXO1 axis.* 2022. 23(1): p. 76-88.
24. Shang, A., et al., *Exosomal miR-183-5p promotes angiogenesis in colorectal cancer by regulation of FOXO1.* Aging (Albany NY), 2020. 12(9): p. 8352-8371.
25. Liu, Z., D. Du, and S. Zhang, *Tumor-derived exosomal miR-1247-3p promotes angiogenesis in bladder cancer by targeting FOXO1.* 2024. 25(1): p. 2290033.
26. Darido, C. and S.M. Jane, *Grhl3 and GEF19 in the front rho.* Small GTPases, 2010. 1(2): p. 104-107.
27. Darido, C., et al., *Targeting of the tumor suppressor GRHL3 by a miR-21-dependent proto-oncogenic network results in PTEN loss and tumorigenesis.* Cancer Cell, 2011. 20(5): p. 635-48.
28. Guardiola-Serrano, F., et al., *Gene trapping identifies a putative tumor suppressor and a new inducer of cell migration.* Biochem Biophys Res Commun, 2008. 376(4): p. 748-52.
29. Fukuda, R., et al., *Insulin-like growth factor 1 induces hypoxia-inducible factor 1-mediated vascular endothelial growth factor expression, which is dependent on MAP kinase and phosphatidylinositol 3-kinase signaling in colon cancer cells.* J Biol Chem, 2002. 277(41): p. 38205-11.
30. Zhong, H., et al., *Modulation of hypoxia-inducible factor 1alpha expression by the epidermal growth factor/phosphatidylinositol 3-kinase/PTEN/AKT/FRAP pathway in human prostate cancer cells: implications for tumor angiogenesis and therapeutics.* Cancer Res, 2000. 60(6): p. 1541-5.
31. Hellwig-Bürgel, T., et al., *Review: hypoxia-inducible factor-1 (HIF-1): a novel*

transcription factor in immune reactions. J Interferon Cytokine Res, 2005. 25(6): p. 297-310.

32. Kasuno, K., et al., *Nitric oxide induces hypoxia-inducible factor 1 activation that is dependent on MAPK and phosphatidylinositol 3-kinase signaling.* J Biol Chem, 2004. 279(4): p. 2550-8.
33. Li, J., et al., *Nickel compounds act through phosphatidylinositol-3-kinase/Akt-dependent, p70(S6k)-independent pathway to induce hypoxia inducible factor transactivation and Cap43 expression in mouse epidermal Cl41 cells.* Cancer Res, 2004. 64(1): p. 94-101.
34. Mazure, N.M., et al., *Induction of vascular endothelial growth factor by hypoxia is modulated by a phosphatidylinositol 3-kinase/Akt signaling pathway in Ha-ras-transformed cells through a hypoxia inducible factor-1 transcriptional element.* Blood, 1997. 90(9): p. 3322-31.
35. Pore, N., et al., *Akt1 activation can augment hypoxia-inducible factor-1alpha expression by increasing protein translation through a mammalian target of rapamycin-independent pathway.* Mol Cancer Res, 2006. 4(7): p. 471-9.
36. Liu, Z.L., et al., *Angiogenic signaling pathways and anti-angiogenic therapy for cancer.* Signal Transduct Target Ther, 2023. 8(1): p. 198.

551 **Figures and legends**

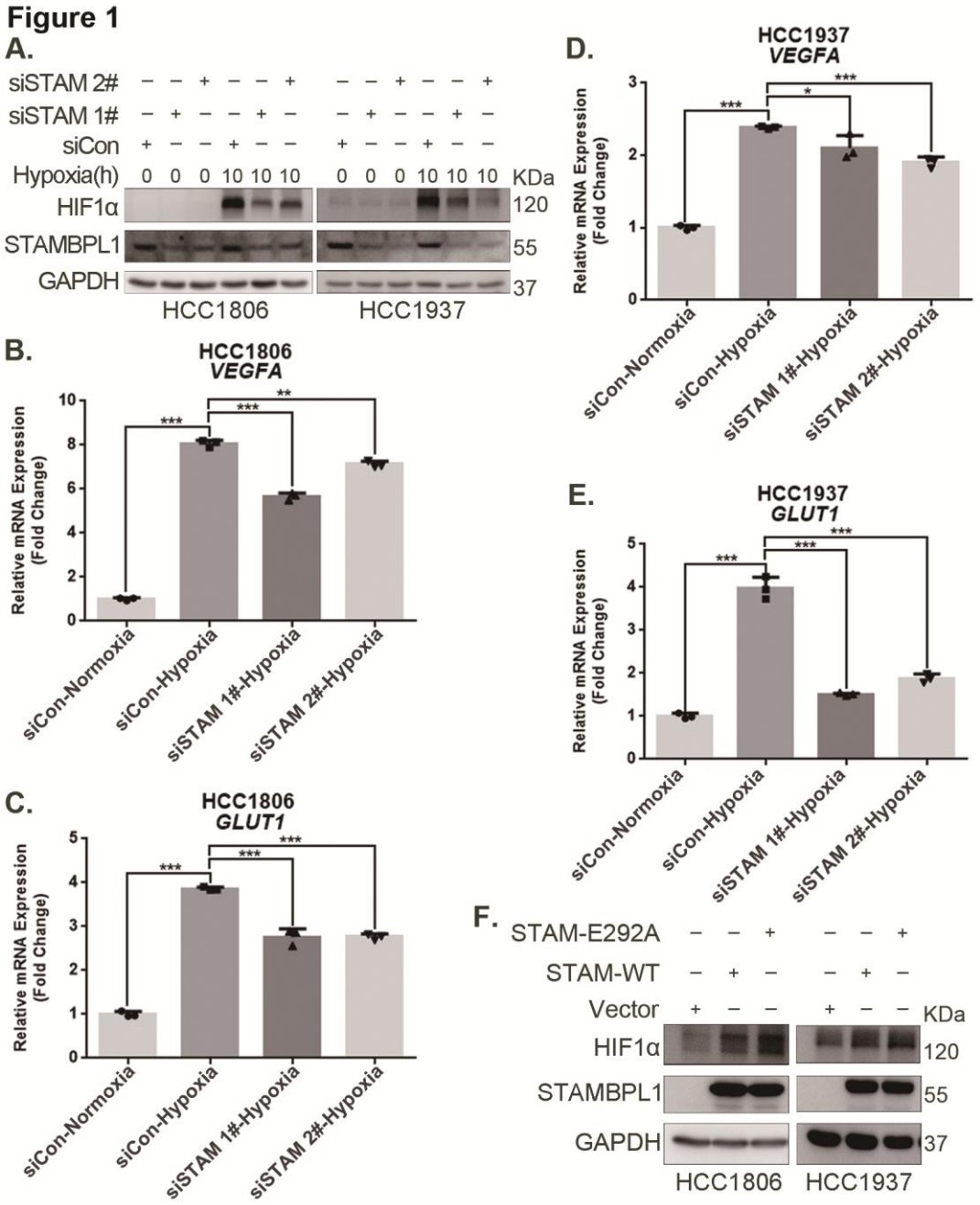

552

553 **Figure 1. STAMBPL1 upregulates HIF1α in a non-enzymatic manner in TNBC cells. (A)**

554 Western blot detected the protein levels of HIF1α when STAMBPL1 was knocked down under

555 normoxia and hypoxia for 10 hours. **(B-C)** RNA samples were collected after 10 h of hypoxia

556 treatment following the knockdown of STAMBPL1 in HCC1806 cells. RT–qPCR experiments

557 were performed to detect the mRNA levels of the HIF1α downstream targets *VEGFA* and

558 *GLUT1*. **(D-E)** RNA samples of HCC1937 were collected as the above HCC1806 cells. RT–

559 qPCR experiments were performed to detect the mRNA levels of the HIF1α downstream targets

560 *VEGFA* and *GLUT1*. **(F)** Western blot detected the protein levels of HIF1α when STAMBPL1

561 /STAMBPL1-E292A was overexpressed under normoxia in HCC1806 and HCC1937 cells. *:

562 $P<0.05$, **: $P<0.01$, ***: $P<0.001$, *t* test.

Figure 2

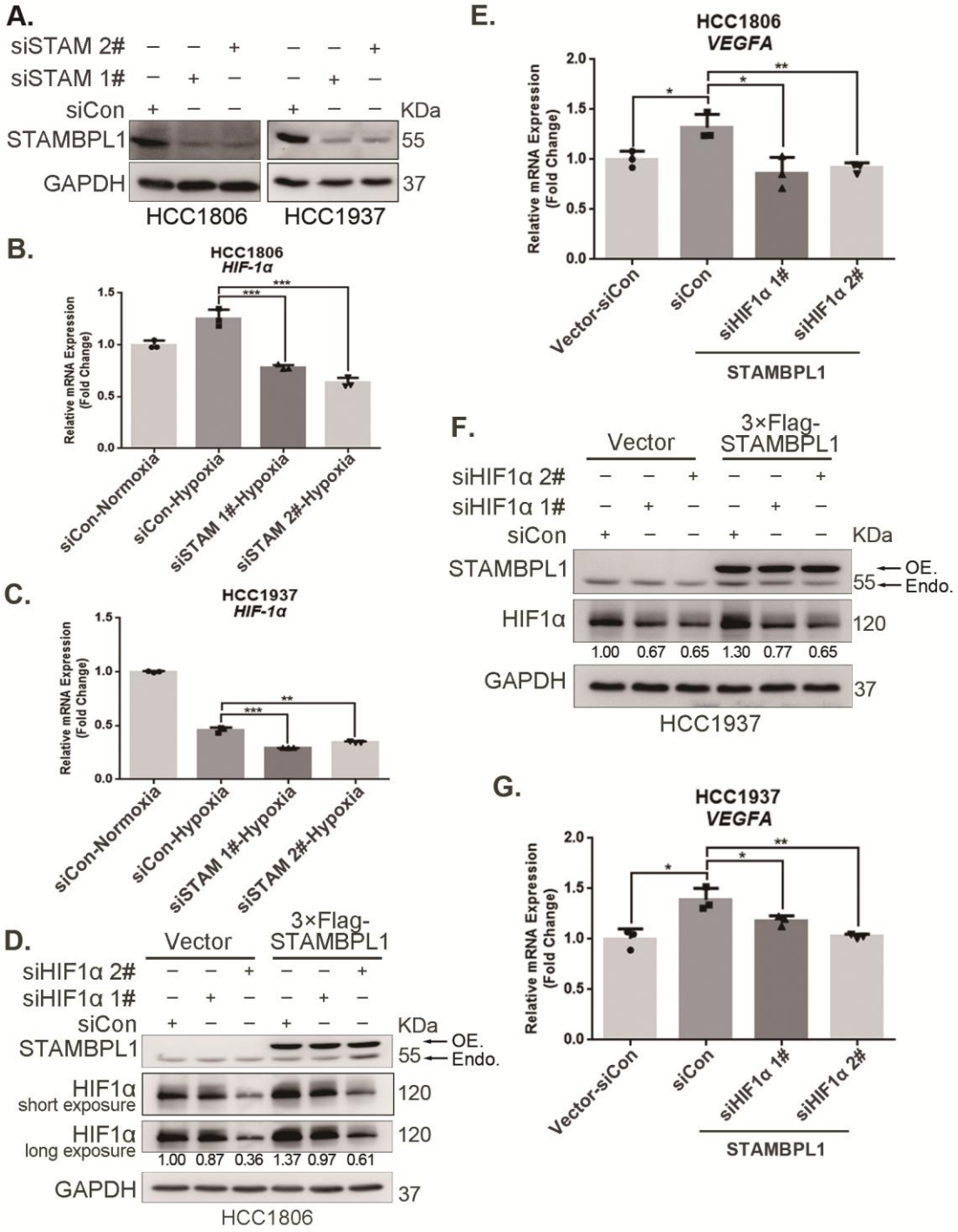
A.
siSTAM 2#
siSTAM 1#
siCon
KDa
STAMBPL1
55
GAPDH
37
HCC1806
HCC1937
B.
HCC1806
HIF-1α
Relative mRNA Expression (Fold Change)
siCon-Normoxia
siCon-Hypoxia
siSTAM 1#-Hypoxia
siSTAM 2#-Hypoxia
C.
HCC1937
HIF-1α
D.
Vector
3×Flag-STAMBPL1
siHIF1α 2#
siHIF1α 1#
siCon
KDa
STAMBPL1
OE.
Endo.
HIF1α short exposure
HIF1α long exposure
1.00 0.87 0.36 1.37 0.97 0.61
GAPDH
HCC1806
E.
HCC1806
VEGFA
Vector-siCon
siCon
siHIF1α 1#
siHIF1α 2#
STAMBPL1
F.
1.00 0.67 0.65 1.30 0.77 0.65
HCC1937
G.
HCC1937
VEGFA

563

564 **Figure 2. STAMBPL1 promotes *HIF1A* transcription and activates the HIF1α/VEGFA axis.**

565 **(A)** Western blot analysis was performed to confirm the knockdown of STAMBPL1 in HCC1806

566 and HCC1937 cells. **(B)** RNA samples were collected after 10 h of hypoxia treatment following

567 the knockdown of STAMBPL1 in HCC1806 cells. RT–qPCR experiments were performed to

568 detect the mRNA levels of HIF1α. **(C)** RNA samples of HCC1937 cells were collected as the

569 above HCC1806 cells. RT–qPCR experiments were performed to detect the mRNA levels of

570 HIF1α. **(D)** Knocking down HIF1α using siRNAs in HCC1806 cells stably overexpressing

571 STAMBPL1 under normoxia. Western blot was used to detect the protein levels of STAMBPL1

572 and HIF1α. **(E)** RT–qPCR experiments were performed to detect the effect of HIF1α knockdown

573 on the mRNA level of *VEGFA* mRNA in HCC1806 cells with STAMBPL1 overexpression under

574 normoxia. **(F)** Knocking down HIF1α using siRNAs in HCC1937 cells stably overexpressing

575 STAMBPL1 under normoxia. Western blot was used to detect the protein levels of STAMBPL1

576 and HIF1α. **(G)** RT–qPCR experiments were performed to detect the effect of HIF1α knockdown

577 on the mRNA level of *VEGFA* mRNA in HCC1937 cells with STAMBPL1 overexpression under

578 normoxia. *: $P<0.05$, **: $P<0.01$, ***: $P<0.001$, *t*-test.

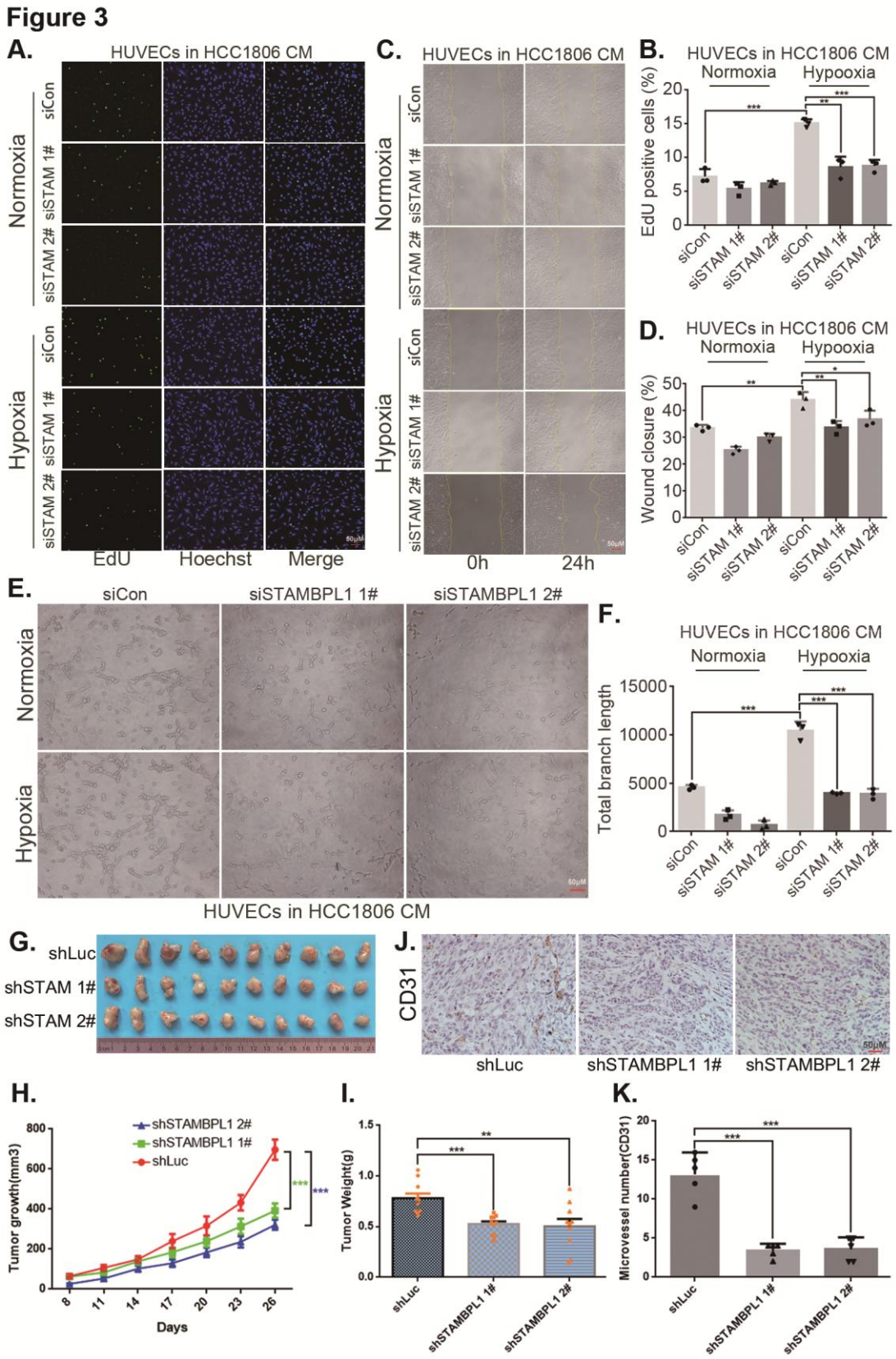

Figure 3. STAMBPL1 in TNBC cells enhances the activity of HUVECs and promotes TNBC angiogenesis. (A) EDU assay was performed to detect the effect of HCC1806 conditioned

582 medium (CM) with STAMBPL1 knockdown under normoxia or hypoxia on the proliferation of
583 HUVECs. **(B)** Statistical analysis of the EdU assay results. **(C)** Wound healing assay was
584 performed to detect the effect of HCC1806 CM with STAMBPL1 knockdown under normoxia or
585 hypoxia on the migration of HUVECs. **(D)** Statistical analysis of the wound healing assay results.
586 **(E)** Tube formation assay was performed to detect the effect of HCC1806 CM with STAMBPL1
587 knockdown under normoxia or hypoxia on the tube formation of HUVECs. **(F)** Statistical
588 analysis of the tube formation assay results. **(G)** The growth of TNBC xenograft tumors was
589 evaluated by photographing the tumors in nude mice to assess the role of STAMBPL1. **(H-I)**
590 The growth and weight of the transplanted tumors in the nude mice were statistically analyzed,
591 and the STAMBPL1sh#1 and STAMBPL1sh#2 groups were compared with the shLuc group.
592 **(J)** An immunohistochemical assay was used to detect the expression of the angiogenesis
593 marker CD31 in xenograft tumors. **(K)** The number of microvessels in the immunohistochemical
594 experiments was statistically analyzed. *: $P<0.05$, **: $P<0.01$, ***: $P<0.001$, *t*-test.

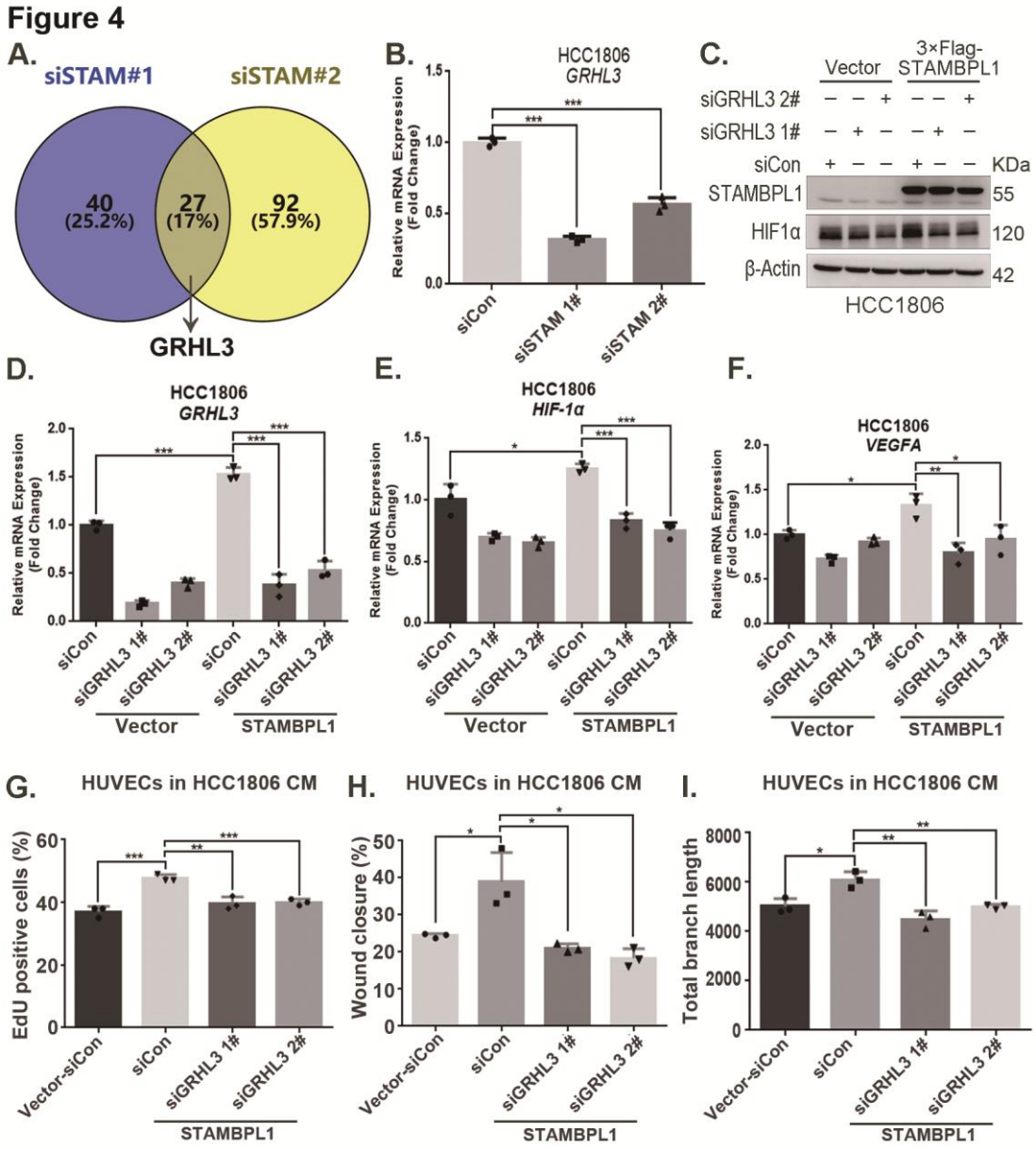

Figure 4. STAMBPL1 promotes *HIF1A* transcription via the upregulation of GRHL3. (A) Venn diagram showing the overlap of differentially expressed genes identified via RNA-seq analysis. **(B)** RT–qPCR experiment was performed to detect the effect of STAMBPL1 knockdown on the mRNA levels of GRHL3 in HCC1806 cells. **(C)** In HCC1806 cells stably overexpressing STAMBPL1, GRHL3 was knocked down via siRNA, after which the protein was collected. Western blotting was performed to detect the effect of GRHL3 knockdown on the expression of HIF1α as STAMBPL1 overexpression under normoxia. **(D-F)** RT–qPCR

603 experiments were performed to detect the knockdown efficiency of GRHL3 and the effect of
604 GRHL3 knockdown on the mRNA levels of HIF1α and its downstream target VEGFA when
605 STAMBPL1 was overexpressing. **(G)** Statistical analysis of the EdU assay results. **(H)** Statistical
606 analysis of the wound healing assay results. **(I)** Statistical analysis of the tube formation assay
607 results. *: $P<0.05$, **: $P<0.01$, ***: $P<0.001$, *t*-test.

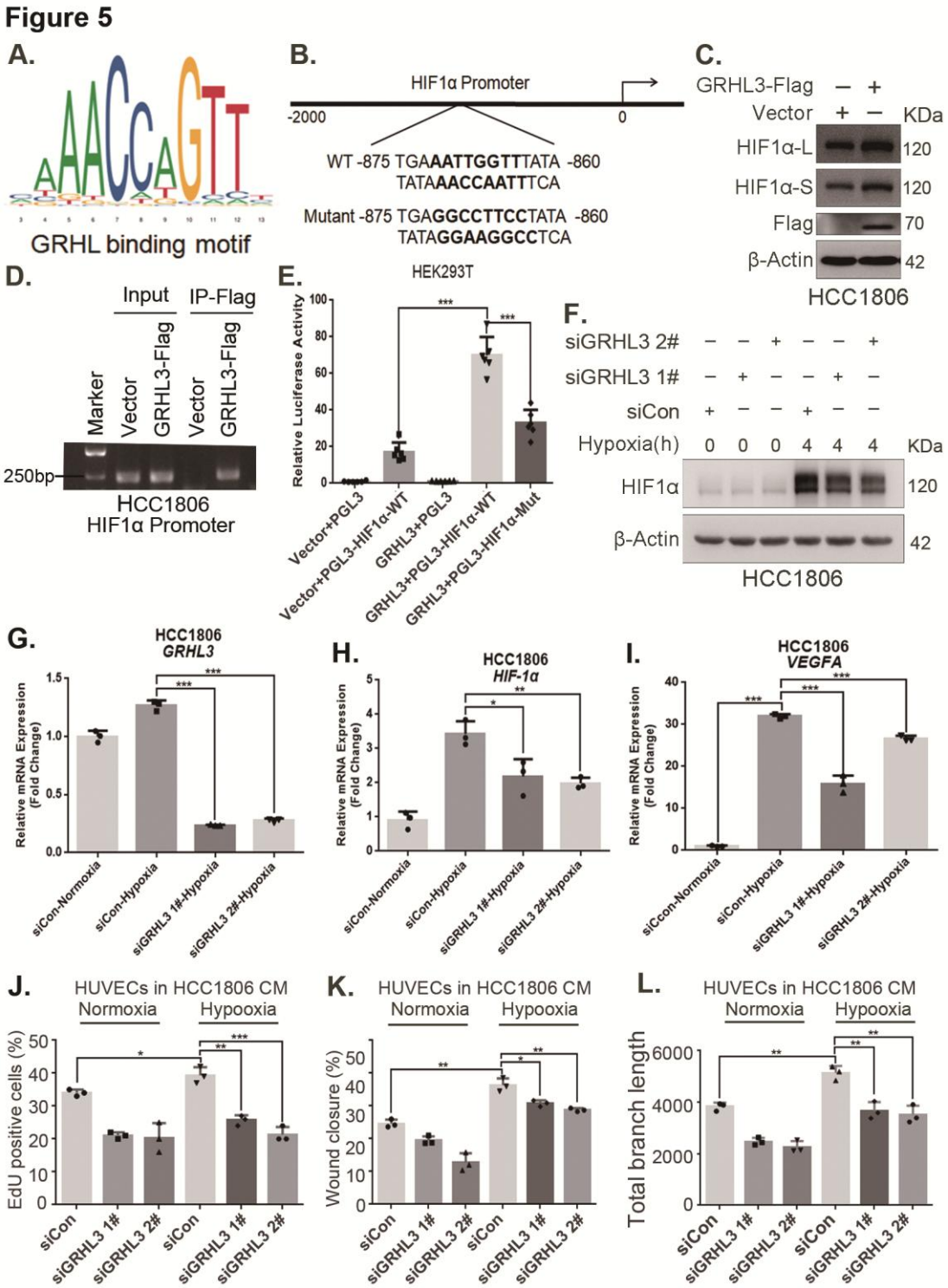

Figure 5. GRHL3 enhances *HIF1A* transcription by binding to its promoter. (A) The JASPAR website was used to predict the potential binding sequence of the transcription factor GRHL3 to the HIF1α promoter. **(B)** Mutation pattern of the HIF1α promoter binding sequence. **(C)** The protein level of HIF1α was detected in HCC1806 cells with GRHL3 overexpression by

613 using Western blot. **(D)** ChIP–PCR experiments conducted in HCC1806 cells stably
614 overexpressing GRHL3 to detect the interaction between GRHL3 and the promoter of *HIF1A*
615 gene. **(E)** A luciferase assay was performed in HEK293T cells to detect the effect of GRHL3 on
616 the transcriptional activity of *HIF1A* promoter. **(F)** In HCC1806 cells, GRHL3 was knocked down
617 by siRNA, and the cells were subjected to hypoxia for 4 hours. Western blotting was performed
618 to detect the effect of GRHL3 knockdown on the protein level of HIF1α. **(G-I)** RT–qPCR
619 experiments were used to detect the effect of GRHL3 knockdown on the mRNA levels of HIF1α
620 and its downstream target VEGFA. **(J)** In HCC1806 cells, GRHL3 was knocked down via siRNA,
621 and the cells were then subjected to hypoxia for 24 hours. The conditioned medium was
622 collected and used to treat HUVECs. EdU assays were performed to detect the effect of GRHL3
623 knockdown CM on the proliferation of HUVECs. Statistical analysis of the EdU assay results
624 was performed. **(K)** Wound healing assays were performed to detect the effect of GRHL3
625 knockdown CM on the migration of HUVECs. Statistical analysis of the wound healing assay
626 results was performed. **(L)** The tube formation assay was performed to detect the effect of
627 GRHL3 knockdown CM on the tube formation of HUVECs. Statistical analysis of the tube
628 formation assay results was performed. *: $P<0.05$, **: $P<0.01$, ***: $P<0.001$, *t*-test.

Figure 6

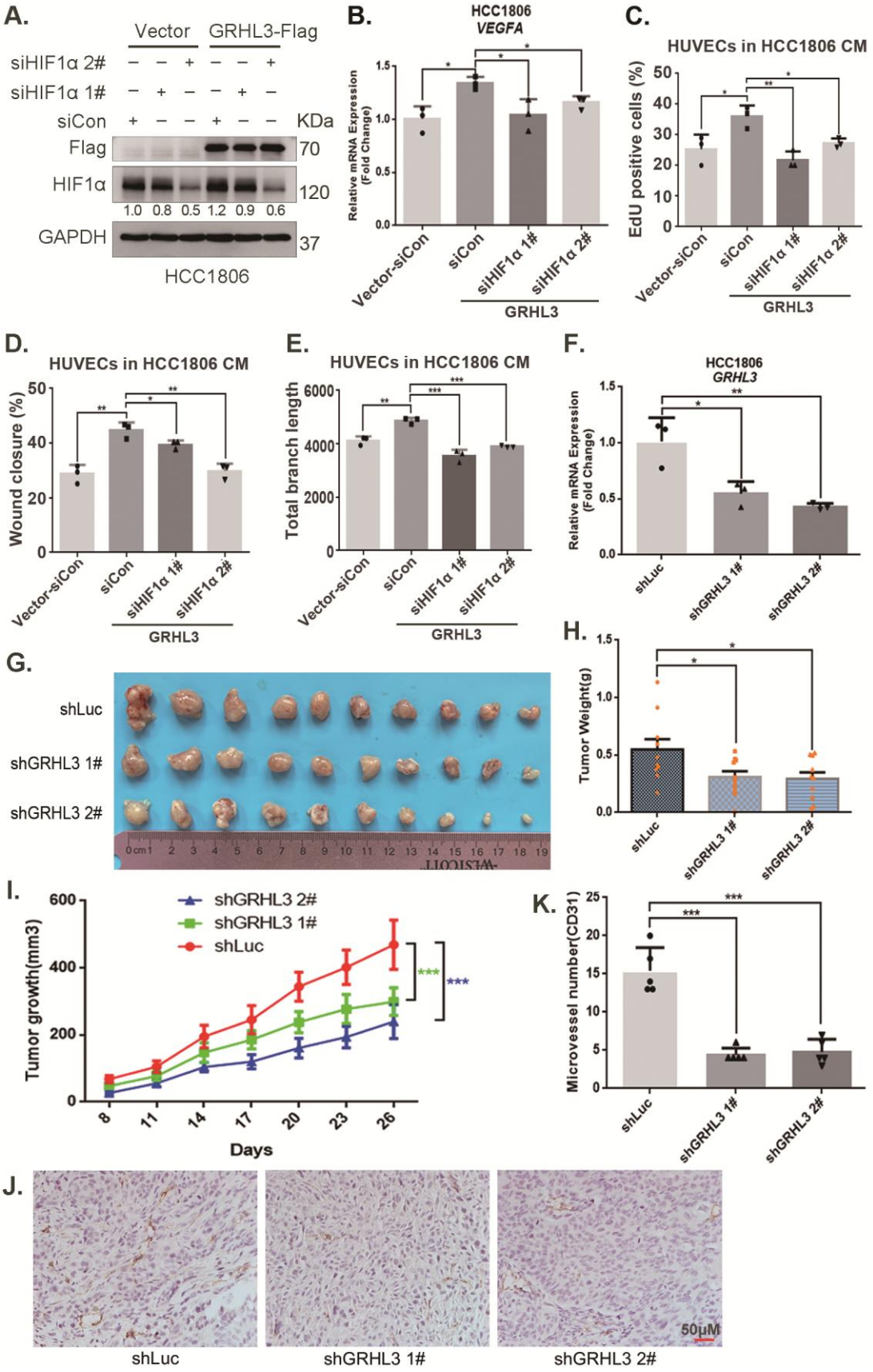
A.
Vector
GRHL3-Flag
siHIF1α 2#
siHIF1α 1#
siCon
KDa
Flag
HIF1α
GAPDH
70
120
37
1.0 0.8 0.5 1.2 0.9 0.6
HCC1806
B.
HCC1806
VEGFA
Relative mRNA Expression (Fold Change)
Vector-siCon
siCon
siHIF1α 1#
siHIF1α 2#
GRHL3
C.
HUVECs in HCC1806 CM
EdU positive cells (%)
D.
HUVECs in HCC1806 CM
Wound closure (%)
E.
HUVECs in HCC1806 CM
Total branch length
F.
HCC1806
GRHL3
shLuc
shGRHL3 1#
shGRHL3 2#
G.
H.
Tumor Weight(g)
I.
Tumor growth(mm3)
Days
K.
Microvessel number(CD31)
J.
50μM

629

630 **Figure 6. GRHL3 enhances *HIF1A* transcription by binding to its promoter. (A)** In
631 HCC1806 cells stably overexpressing GRHL3, HIF1α was knocked down by siRNA, and the
632 protein was subsequently collected. Western blotting was performed to detect the protein level
633 of GRHL3-Flag and HIF1α. **(B)** RT–qPCR experiments were performed to detect the effect of
634 HIF1α knockdown on the mRNA level of VEGFA as GRHL3 overexpression. **(C)** HCC1806 cells
635 stably overexpressing GRHL3 were used for the knockdown of HIF1α via siRNA. The
636 conditioned medium was then collected and used to treat HUVECs. EdU assay was performed
637 to detect the effect of CM with HIF1α knockdown on the proliferation of HUVECs as GRHL3
638 overexpression. **(D)** Wound healing assay was performed to detect the effect of CM with HIF1α
639 knockdown on the migration of HUVECs as GRHL3 overexpression. **(E)** The tube formation
640 assay was performed to detect the effect of CM with HIF1α knockdown on the tube formation
641 of HUVECs as GRHL3 overexpression. **(F)** RT–qPCR was used to detect the knockdown of
642 GRHL3 in HCC1806 cells. **(G)** Photographs of xenograft tumors from nude mice were taken to
643 evaluate the role of GRHL3 in the growth of TNBC xenograft tumors. **(H)** The weights of the
644 transplanted tumors from the nude mice were statistically analyzed, and the shGRHL3 1# and
645 shGRHL3 2# groups were compared with the shLuc group. **(I)** The growth of transplanted
646 tumors in nude mice was statistically analyzed, and the shGRHL3 1# and shGRHL3 2# groups
647 were compared with the shLuc group. **(J)** An immunohistochemical assay was performed to
648 detect the expression of the angiogenesis marker CD31 in xenograft tumors. **(K)** Statistical
649 analysis of the number of microvessels in the immunohistochemical experiments. *: $P<0.05$, **:
650 $P<0.01$, ***: $P<0.001$, *t*-test.

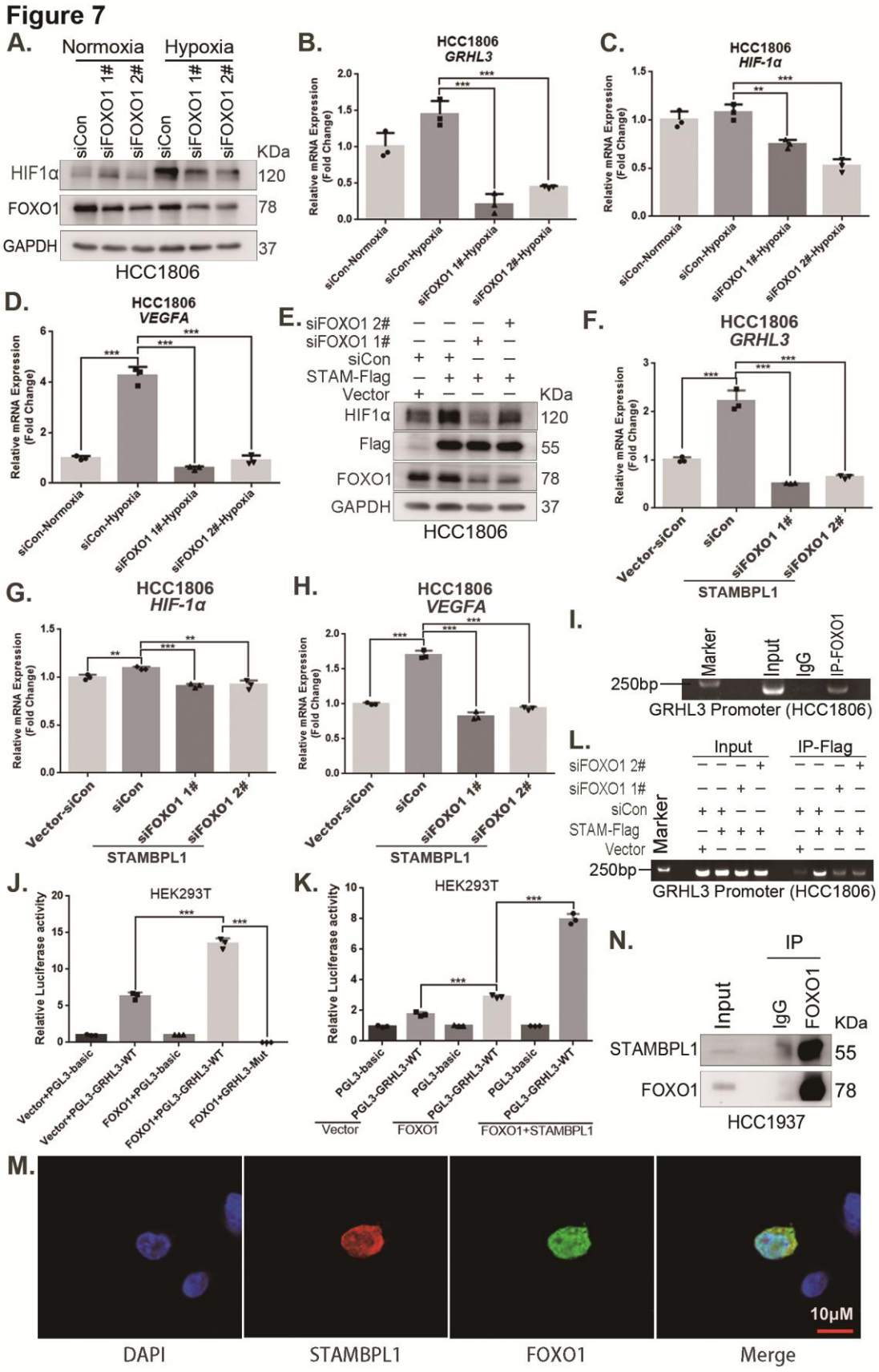
Figure 7
A.
Normoxia
Hypoxia
siCon
siFOXO1 1#
siFOXO1 2#
KDa
HIF1α
FOXO1
GAPDH
120
78
37
HCC1806
B.
HCC1806
GRHL3
Relative mRNA Expression (Fold Change)
siCon-Normoxia
siCon-Hypoxia
siFOXO1 1#-Hypoxia
siFOXO1 2#-Hypoxia
C.
HCC1806
HIF-1α
D.
HCC1806
VEGFA
E.
siFOXO1 2#
siFOXO1 1#
siCon
STAM-Flag
Vector
Flag
55
F.
HCC1806
GRHL3
Vector-siCon
STAMBPL1
G.
HCC1806
HIF-1α
H.
HCC1806
VEGFA
I.
Marker
Input
IgG
IP-FOXO1
250bp
GRHL3 Promoter (HCC1806)
L.
Input
IP-Flag
J.
HEK293T
Relative Luciferase activity
Vector+PGL3-basic
Vector+PGL3-GRHL3-WT
FOXO1+PGL3-basic
FOXO1+PGL3-GRHL3-WT
FOXO1+GRHL3-Mut
K.
PGL3-basic
PGL3-GRHL3-WT
Vector
FOXO1
FOXO1+STAMBPL1
N.
IP
STAMBPL1
HCC1937
M.
10μM
DAPI
STAMBPL1
FOXO1
Merge

651

Figure 7. STAMBPL1 mediates *GRHL3* transcription by interacting with FOXO1. (A) Western blotting was used to detect the HIF1α protein expression when FOXO1 was knocking down in HCC1806 cells followed by hypoxia treatment for 4 hours. **(B-D)** RT–qPCR experiments were performed to detect the effect of FOXO1 knockdown on the mRNA levels of GRHL3/HIF1α/VEGFA in HCC1806 cells under hypoxia for 4 hours. **(E)** In HCC1806 cells stably overexpressing STAMBPL1, protein samples were collected after FOXO1 was knocked down via siRNA. Western blotting was performed to detect the effect of FOXO1 knockdown on the expression of HIF1α as STAMBPL1 overexpression. **(F-H)** RT–qPCR experiments were performed to detect the effect of FOXO1 knockdown on the mRNA expression of GRHL3, HIF1α and VEGFA as STAMBPL1 overexpression. **(I)** An endogenous ChIP–PCR assay was performed using an anti-FOXO1 antibody in HCC1806 cells. **(J)** A luciferase assay was performed in HEK293T cells to detect the effect of FOXO1 on the transcriptional activity of GRHL3 promoter. **(K)** A luciferase assay was conducted in HEK293T cells to detected the effect of STAMBPL1 on the activation of the GRHL3 promoter by FOXO1. **(L)** ChIP–PCR experiments were performed in HCC1806 cells stably overexpressing STAMBPL1 after knocking down FOXO1 via siRNA. **(M)** PCDH-STAMBPL1-3×Flag and PCDH-FOXO1-3×Flag plasmids were co-transfected into HEK293T cells, and then, immunofluorescence experiments were performed. Red represents STAMBPL1 staining, green represents FOXO1 staining, and blue represents DAPI staining. **(N)** Endogenous STAMBPL1 protein was immunoprecipitated from HCC1937 cells via an anti-FOXO1 antibody. Immunoglobulin G (IgG) served as the negative control. Endogenous STAMBPL1 was detected via western blotting. *: $P<0.05$, **: $P<0.01$, ***: $P<0.001$, *t*-test.

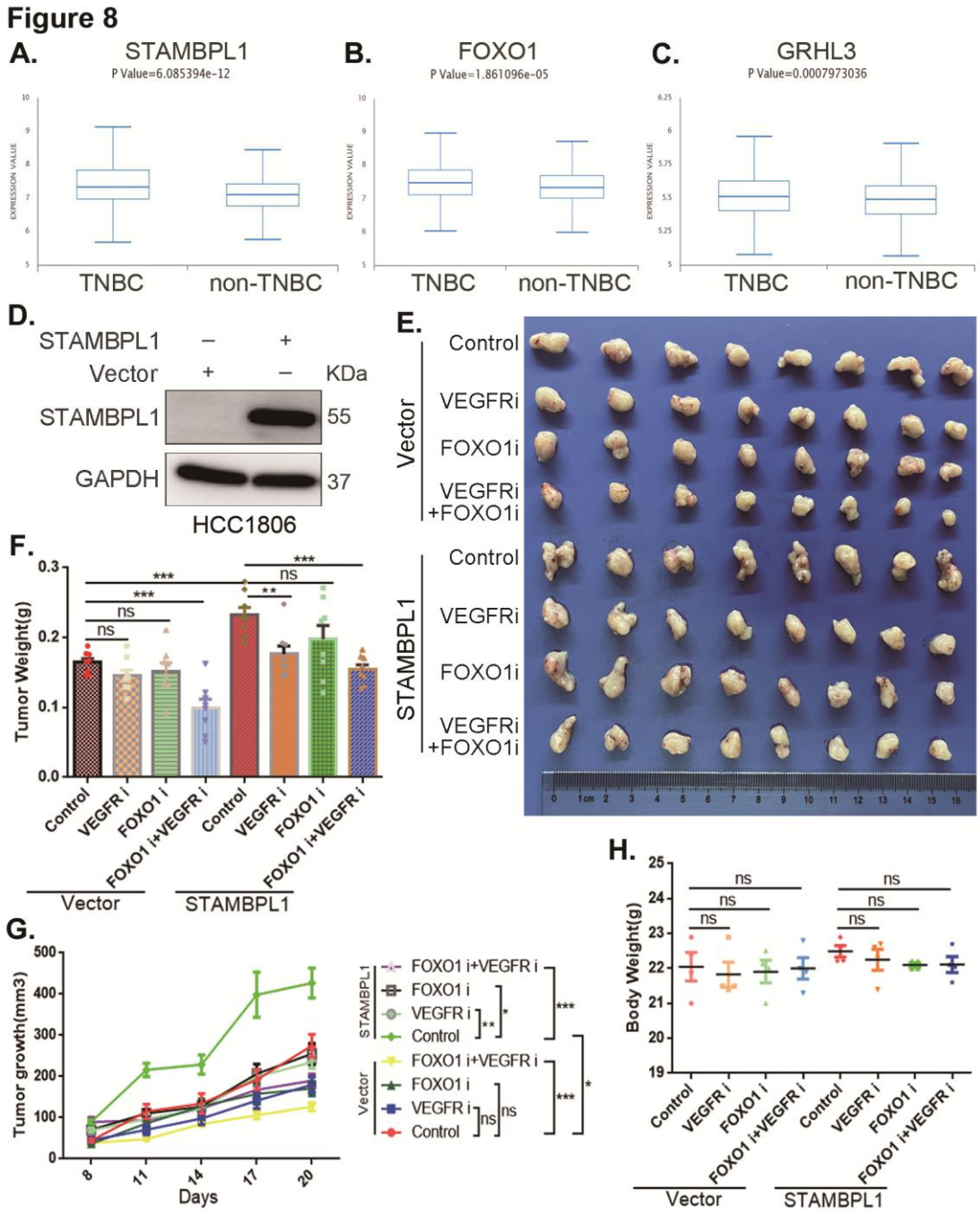

674

675 **Figure 8. The combination of VEGFR and FOXO1 inhibitors synergistically suppresses**

676 **TNBC xenograft growth. (A-C)** Metabric database analysis in BCIP revealed high expression

677 levels of STAMBPL1, FOXO1, and GRHL3 in TNBC (n = 319) compared with non-TNBC (n =

678 1661). **(D)** The effect of STAMBPL1 overexpression in HCC1806 cells was detected by Western

679 blotting. **(E)** Nude mice with tumors received the FOXO1 inhibitor AS1842856 (10 mg/kg, every

680 two days) or the VEGFR inhibitor Apatinib (50 mg/kg, every two days) or a combination of both

treatments. The effect of the drug treatments on the transplanted tumors was assessed by imaging the tumors. **(F-G)** The weight and growth of the transplanted tumors in the nude mice were statistically analyzed. The vector control group and the STAMBPL overexpression group were compared. The nondrug group and the combined drug group in the vector control group were compared. The nondrug group and the combined drug group in the STAMBPL overexpression group were compared. **(H)** The final weights of the nude mice were statistically analyzed. *: *P*<0.05, **: *P*<0.01, ***: *P*<0.001, *t*-test.

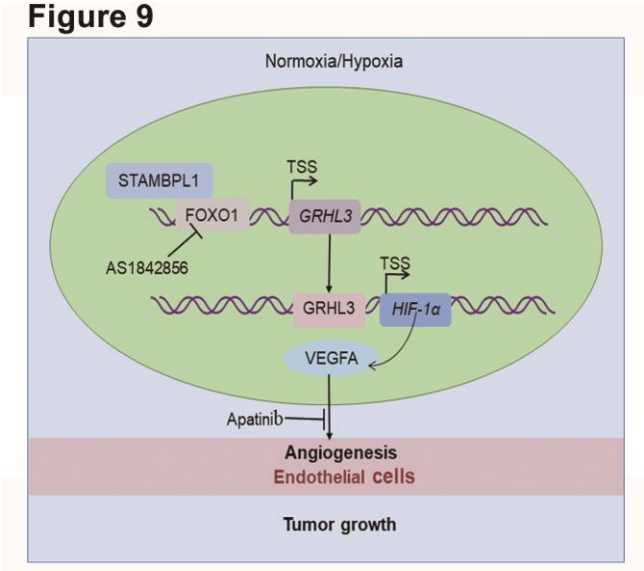

Figure 9. The working model of this study. STAMBPL1 interacts with FOXO1 to promote TNBC angiogenesis by activating the GRHL3/HIF1α/VEGFA axis.

Additional material

Supplementary Material 1

Figure S1. STAMBPL1 in TNBC cells enhances the activity of HUVECs. (A) EDU assay was performed to detect the effect of HCC1937 CM with STAMBPL1 knockdown under normoxia or hypoxia on the proliferation of HUVECs. **(B)** Statistical analysis of the EdU assay

697 results. **(C)** Wound healing assay was performed to detect the effect of HCC1937 CM with
698 STAMBPL1 knockdown under normoxia or hypoxia on the migration of HUVECs. **(D)** Statistical
699 analysis of the wound healing assay results. **(E)** Tube formation assay was performed to detect
700 the effect of HCC1937 CM with STAMBPL1 knockdown under normoxia or hypoxia on the tube
701 formation of HUVECs. **(F)** Statistical analysis of the tube formation assay results. *: $P<0.05$, **:
702 $P<0.01$, ***: $P<0.001$, *t*-test.

703 **Figure S2. STAMBPL1 in TNBC cells enhances the activity of HUVECs. (A and D)**
704 HCC1806 and HCC1937 cells were stably overexpressing STAMBPL1, and HIF1α was
705 knocked down using siRNA. The conditioned medium was then collected and used to treat
706 HUVECs. EdU assay was performed to detect the effect of CM with HIF1α knockdown on the
707 proliferation of HUVECs as STAMBPL1 overexpression. Statistical analysis of the EdU assay
708 results was performed. **(B and E)** Wound healing assay was performed to detect the effect of
709 CM with HIF1α knockdown on the migration of HUVECs as STAMBPL1 overexpression.
710 Statistical analysis of the wound healing assay results was performed. **(C and F)** Tube
711 formation assay was performed to detect the effect of CM with HIF1α knockdown on the tube
712 formation of HUVECs as STAMBPL1 overexpression. Statistical analysis of the tube formation
713 assay results was performed. *: $P<0.05$, **: $P<0.01$, ***: $P<0.001$, *t*-test.

714 **Figure S3. STAMBPL1 promotes *HIF1A* transcription via upregulating GRHL3. (A)** RNA-
715 seq result: the list of 18 genes downregulated after STAMBPL1 knockdown in HCC1806 cells.
716 **(B)** RT-qPCR experiments showed that knockdown of STAMBPL1 inhibited GRHL3 mRNA
717 levels in HCC1937 cells. **(C)** In HCC1937 cells stably overexpressing STAMBPL1, GRHL3 was
718 knocked down using siRNA, and then the protein was collected. Western blotting was

719 performed to detect the effect of GRHL3 knockdown on the expression of HIF1α as
720 STAMBPL1overexpression. **(D-F)** RT-qPCR experiments were performed to detect the
721 knockdown efficiency of GRHL3 and the effect of GRHL3 knockdown on the mRNA levels of
722 HIF1α and its downstream target VEGFA when STAMBPL1 was overexpressing. **(G)** Statistical
723 analysis of EdU assay. **(H)** Statistical analysis of wound healing assay. **(I)** Statistical analysis of
724 tube formation assay. *: $P<0.05$, **: $P<0.01$, ***: $P<0.001$, *t*-test.

725 **Figure S4. GRHL3 enhances *HIF1A* transcription by binding to its promoter. (A)** In
726 HCC1937 cells, knockdown of GRHL3 using siRNA and treated with hypoxia for 4 hours.
727 Western blotting was performed to detect the effect of GRHL3 knockdown on the protein level
728 of HIF1α. **(B-D)** RT-qPCR experiments were performed to detect the knockdown efficiency of
729 GRHL3 and the effect of GRHL3 knockdown on the mRNA levels of HIF1α and its downstream
730 target VEGFA. **(E)** In HCC1937 cells, GRHL3 was knocked down by siRNA and then treated
731 with hypoxia for 24 hours, and then the conditioned medium was collected to treat HUVECs,
732 EdU assay was performed to detect the effect of the CM with GRHL3 knockdown on the
733 proliferation of HUVECs. **(F)** Wound healing assay was performed to detect the effect of the
734 CM with GRHL3 knockdown on the migration of HUVECs. **(G)** The tube formation assay was
735 performed to detect the effect of the CM with GRHL3 knockdown on the tube formation of
736 HUVECs. **(H)** In HCC1937 cells stably overexpressing GRHL3, HIF1α was knocked down using
737 siRNA, and then the protein was collected. Western blotting was performed to detect the protein
738 levels of GRHL3 and HIF1α. **(I)** RT-qPCR experiment was performed to detect the effect of
739 HIF1α knockdown on the mRNA expression of VEGFA as GRHL3 overexpression. **(J)**
740 Statistical analysis of EdU assay results. **(K)** Statistical analysis of wound healing assay results.

741 **(L)** Statistical analysis of tube formation assay results. *: *P*<0.05, **: *P*<0.01, ***: *P*<0.001, *t*-
742 test.

743 **Figure S5. STAMBPL1 mediates *GRHL3* transcription by interacting with FOXO1. (A)**
744 Western blotting was performed to detect the effect of FOXO1 knockdown on the protein level
745 of HIF1α in HCC1937 cells under hypoxia for 4 hours. **(B-D)** RT-qPCR experiments were
746 performed to detect the effect of FOXO1 knockdown on the mRNA levels of
747 GRHL3/HIF1α/VEGFA in HCC1937 cells under hypoxia treatment for 4 hours. **(E)** Western blot
748 detected the FOXO1 expression when STAMBPL1 and STAMPBL1-E292A were
749 overexpressed. **(F)** The JASPAR website predicts the possible binding sequence of
750 transcription factor FOXO1 to the GRHL3 promoter and its mutation pattern map. **(G)** The
751 truncated structure diagram of STAMBPL1. **(H)** The truncated structure diagram of FOXO1. **(I)**
752 The full-length and truncated plasmids of pEBG-STAMBPL1-GST and pCDH-FOXO1-no tag
753 were transfected into HEK293T cells, and the proteins were collected for GST-pull down assay
754 at 48 hours after transfection. **(J)** The full-length and truncated plasmids of pCDH-FOXO1-
755 3×Flag and pEBG-STAMBPL1-GST were transfected into HEK293T cells, and the proteins
756 were collected for IP-Flag assay at 48 hours after transfection. *: *P*<0.05, **: *P*<0.01, ***:
757 *P*<0.001, *t* -test.

758 **Figure S6. STAMBPL1, FOXO1, and GRHL3 is highly expressed in TNBC. (A-C)** The
759 expression of STAMBPL1, FOXO1, and GRHL3 in adjacent normal of TNBC (n=29), TNBC
760 (n=319), adjacent normal of non-TNBC (n=102), and non-TNBC (n=1661) by analyzing the
761 Metabric database in BCIP. **(D)** The mutation, amplification, and deep deletion of STAMBPL1

762 in breast cancer were analyzed by using cBioportal online database. **(E)** The expression of

763 STAMBPL1 in non-TNBC and subtypes of TNBC by using bc-GenExMiner online database.

Figure 1

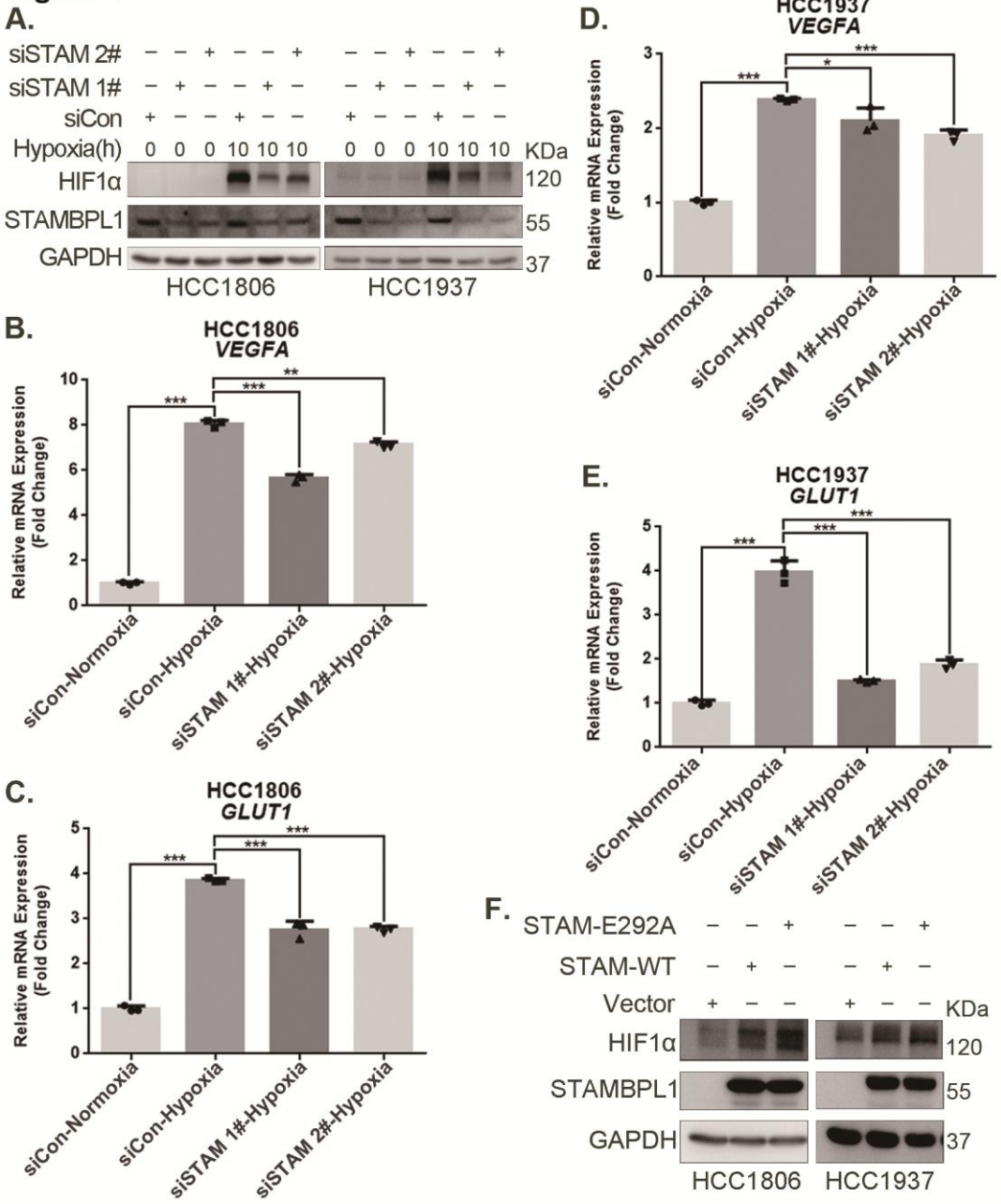
A.
siSTAM 2#
siSTAM 1#
siCon
Hypoxia(h)
0 0 0 10 10 10
0 0 0 10 10 10
KDa
HIF1α
STAMBPL1
GAPDH
120
55
37
HCC1806
HCC1937
B.
HCC1806
VEGFA
C.
HCC1806
GLUT1
D.
HCC1937
VEGFA
E.
HCC1937
GLUT1
Relative mRNA Expression (Fold Change)
siCon-Normoxia
siCon-Hypoxia
siSTAM 1#-Hypoxia
siSTAM 2#-Hypoxia
F.
STAM-E292A
STAM-WT
Vector
KDa
HIF1α
STAMBPL1
GAPDH
120
55
37
HCC1806
HCC1937

Figure 2

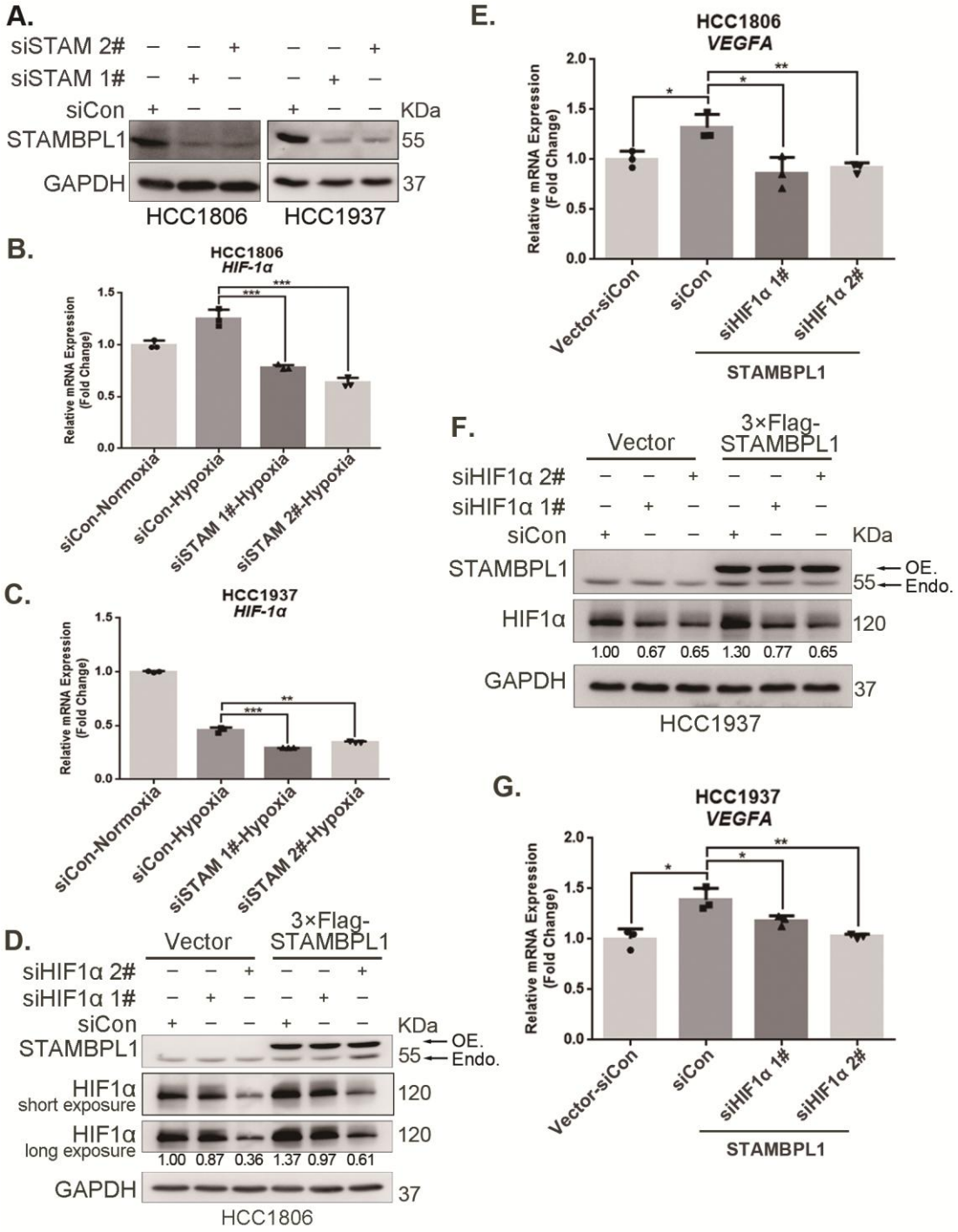
A.
siSTAM 2#
siSTAM 1#
siCon
KDa
STAMBPL1
55
GAPDH
37
HCC1806
HCC1937
B.
HCC1806
HIF-1α
Relative mRNA Expression (Fold Change)
siCon-Normoxia
siCon-Hypoxia
siSTAM 1#-Hypoxia
siSTAM 2#-Hypoxia
C.
HCC1937
HIF-1α
D.
Vector
3×Flag-STAMBPL1
siHIF1α 2#
siHIF1α 1#
siCon
KDa
STAMBPL1
OE.
Endo.
HIF1α short exposure
HIF1α long exposure
120
1.00 0.87 0.36 1.37 0.97 0.61
GAPDH
HCC1806
E.
HCC1806
VEGFA
Vector-siCon
siCon
siHIF1α 1#
siHIF1α 2#
STAMBPL1
F.
1.00 0.67 0.65 1.30 0.77 0.65
HCC1937
G.
HCC1937
VEGFA

Figure 3

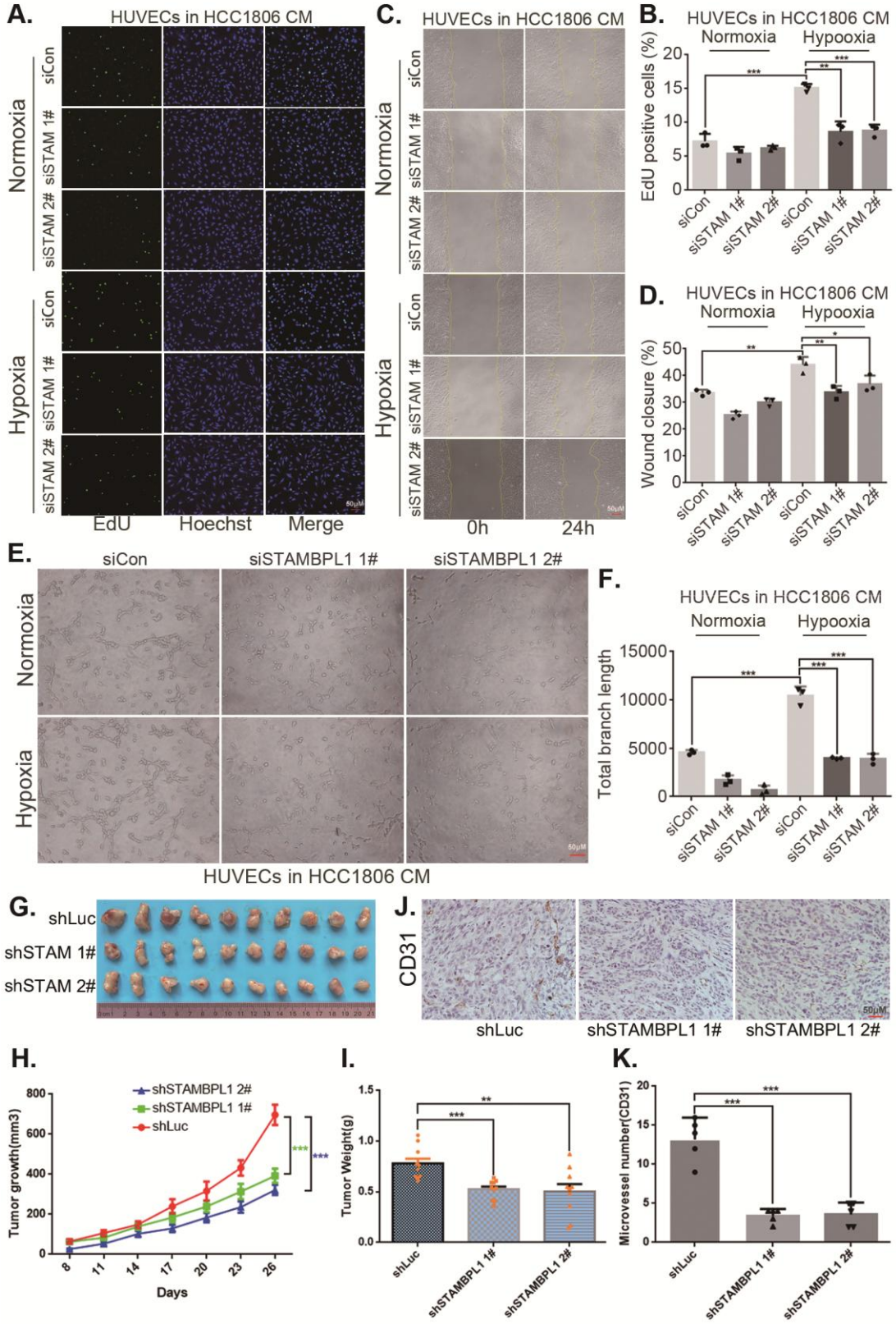
A.
HUVECs in HCC1806 CM
Normoxia
Hypoxia
siCon
siSTAM 1#
siSTAM 2#
EdU
Hoechst
Merge
C.
HUVECs in HCC1806 CM
0h
24h
B.
HUVECs in HCC1806 CM
Normoxia
Hypooxia
EdU positive cells (%)
D.
HUVECs in HCC1806 CM
Wound closure (%)
E.
siCon
siSTAMBPL1 1#
siSTAMBPL1 2#
HUVECs in HCC1806 CM
F.
HUVECs in HCC1806 CM
Total branch length
G.
shLuc
shSTAM 1#
shSTAM 2#
J.
CD31
shLuc
shSTAMBPL1 1#
shSTAMBPL1 2#
H.
shSTAMBPL1 2#
shSTAMBPL1 1#
shLuc
Tumor growth(mm3)
Days
I.
Tumor Weight(g)
K.
Microvessel number(CD31)

Figure 4

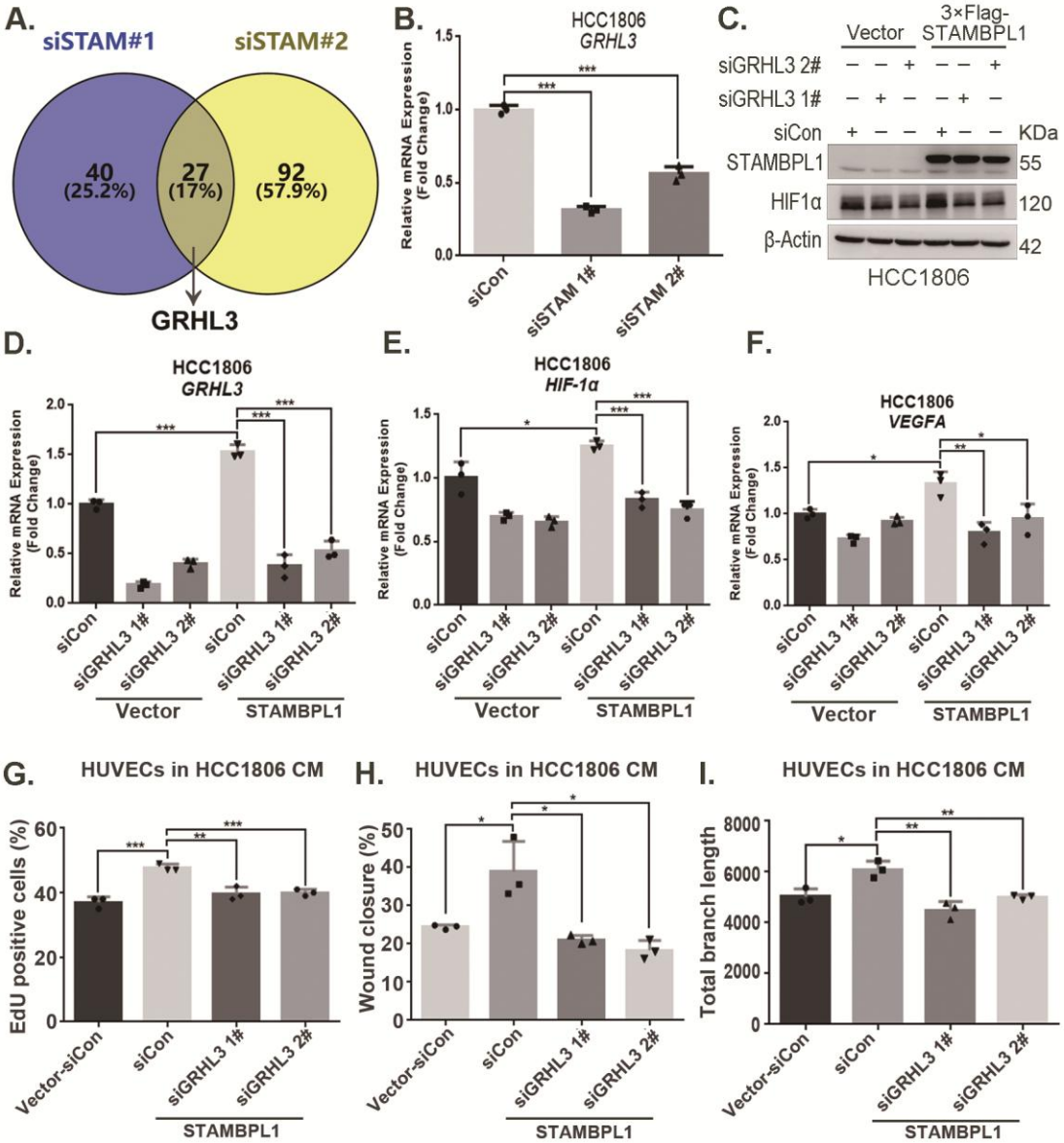
A.
siSTAM#1
siSTAM#2
40 (25.2%)
27 (17%)
92 (57.9%)
GRHL3
B.
HCC1806
GRHL3
Relative mRNA Expression (Fold Change)
siCon
siSTAM 1#
siSTAM 2#
C.
Vector
3×Flag-STAMBPL1
siGRHL3 2#
siGRHL3 1#
siCon
KDa
STAMBPL1
HIF1α
β-Actin
55
120
42
HCC1806
D.
HCC1806
GRHL3
E.
HCC1806
HIF-1α
F.
HCC1806
VEGFA
siGRHL3 1#
siGRHL3 2#
Vector
STAMBPL1
G.
HUVECs in HCC1806 CM
EdU positive cells (%)
Vector-siCon
H.
Wound closure (%)
I.
Total branch length

Figure 5

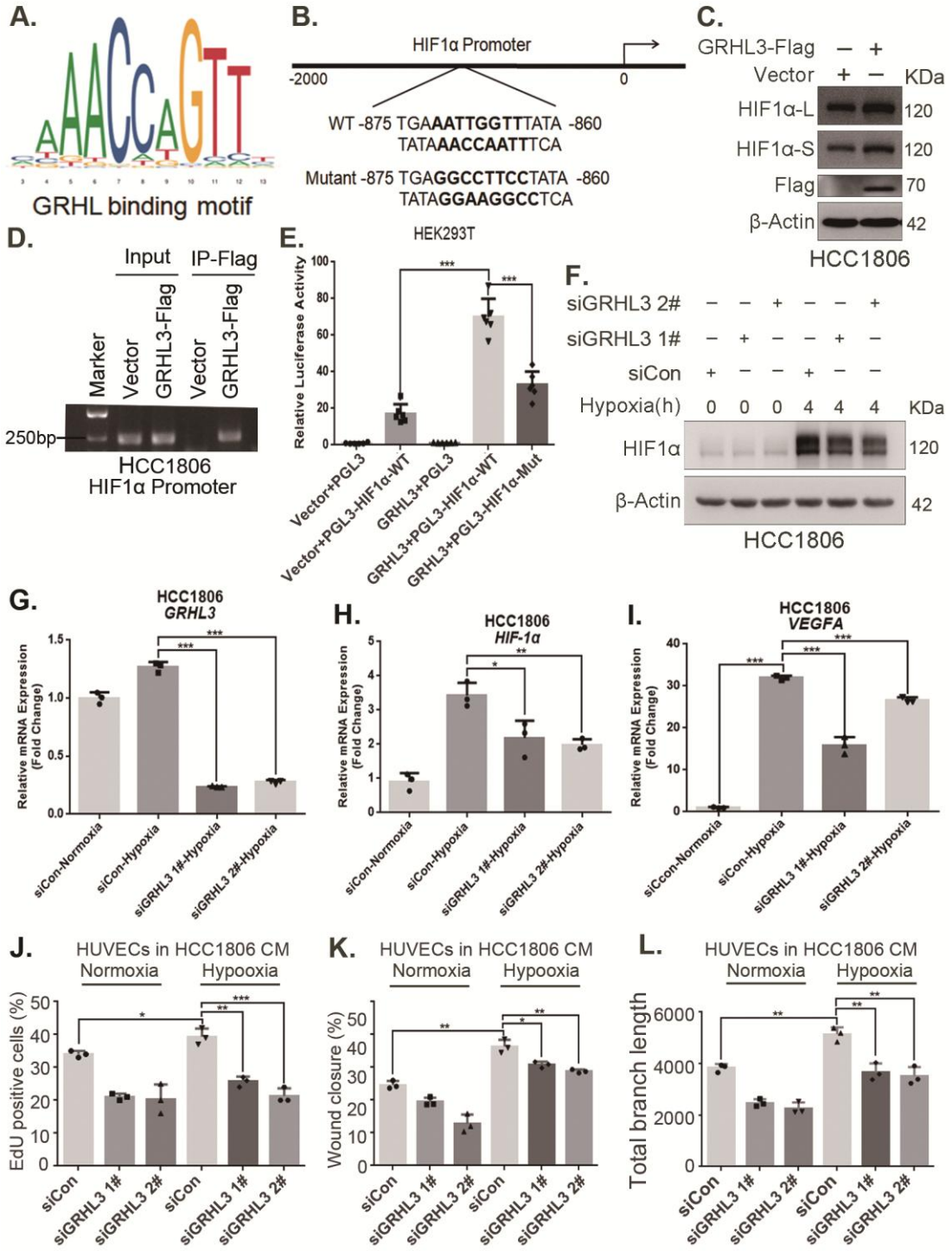
A.
GRHL binding motif
B.
HIF1α Promoter
-2000
0
WT -875 TGAAATTGGTTTATA -860
TATAAACCAATTTCA
Mutant -875 TGAGGCCTTCCTATA -860
TATAGGAAGGCCTCA
C.
GRHL3-Flag
Vector
KDa
HIF1α-L
HIF1α-S
Flag
β-Actin
120
120
70
42
HCC1806
D.
Input
IP-Flag
Marker
Vector
GRHL3-Flag
Vector
GRHL3-Flag
250bp
HCC1806
HIF1α Promoter
E.
HEK293T
Relative Luciferase Activity
Vector+PGL3
Vector+PGL3-HIF1α-WT
GRHL3+PGL3
GRHL3+PGL3-HIF1α-WT
GRHL3+PGL3-HIF1α-Mut
F.
siGRHL3 2#
siGRHL3 1#
siCon
Hypoxia(h)
KDa
HIF1α
β-Actin
120
42
HCC1806
G.
HCC1806
GRHL3
Relative mRNA Expression (Fold Change)
siCon-Normoxia
siCon-Hypoxia
siGRHL3 1#-Hypoxia
siGRHL3 2#-Hypoxia
H.
HCC1806
HIF-1α
I.
HCC1806
VEGFA
J.
HUVECs in HCC1806 CM
Normoxia
Hypooxia
EdU positive cells (%)
siCon
siGRHL3 1#
siGRHL3 2#
K.
Wound closure (%)
L.
Total branch length

Figure 6

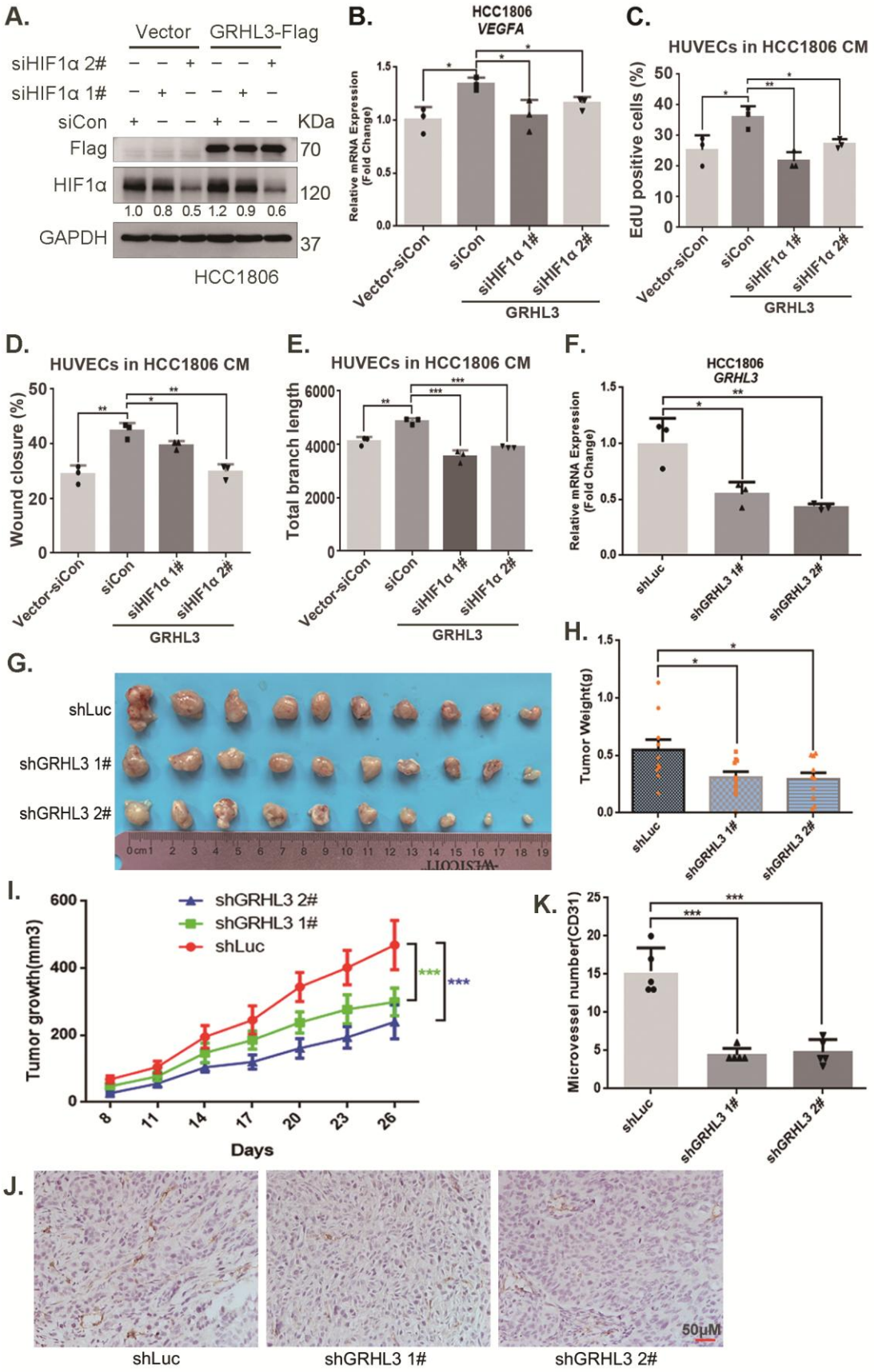
A.
Vector
GRHL3-Flag
siHIF1α 2#
siHIF1α 1#
siCon
KDa
Flag
70
HIF1α
120
1.0 0.8 0.5 1.2 0.9 0.6
GAPDH
37
HCC1806
B.
HCC1806
VEGFA
Relative mRNA Expression (Fold Change)
Vector-siCon
siCon
siHIF1α 1#
siHIF1α 2#
GRHL3
C.
HUVECs in HCC1806 CM
EdU positive cells (%)
D.
HUVECs in HCC1806 CM
Wound closure (%)
E.
HUVECs in HCC1806 CM
Total branch length
F.
HCC1806
GRHL3
shLuc
shGRHL3 1#
shGRHL3 2#
G.
H.
Tumor Weight(g)
I.
Tumor growth(mm3)
Days
K.
Microvessel number(CD31)
J.
50μM

Figure 7

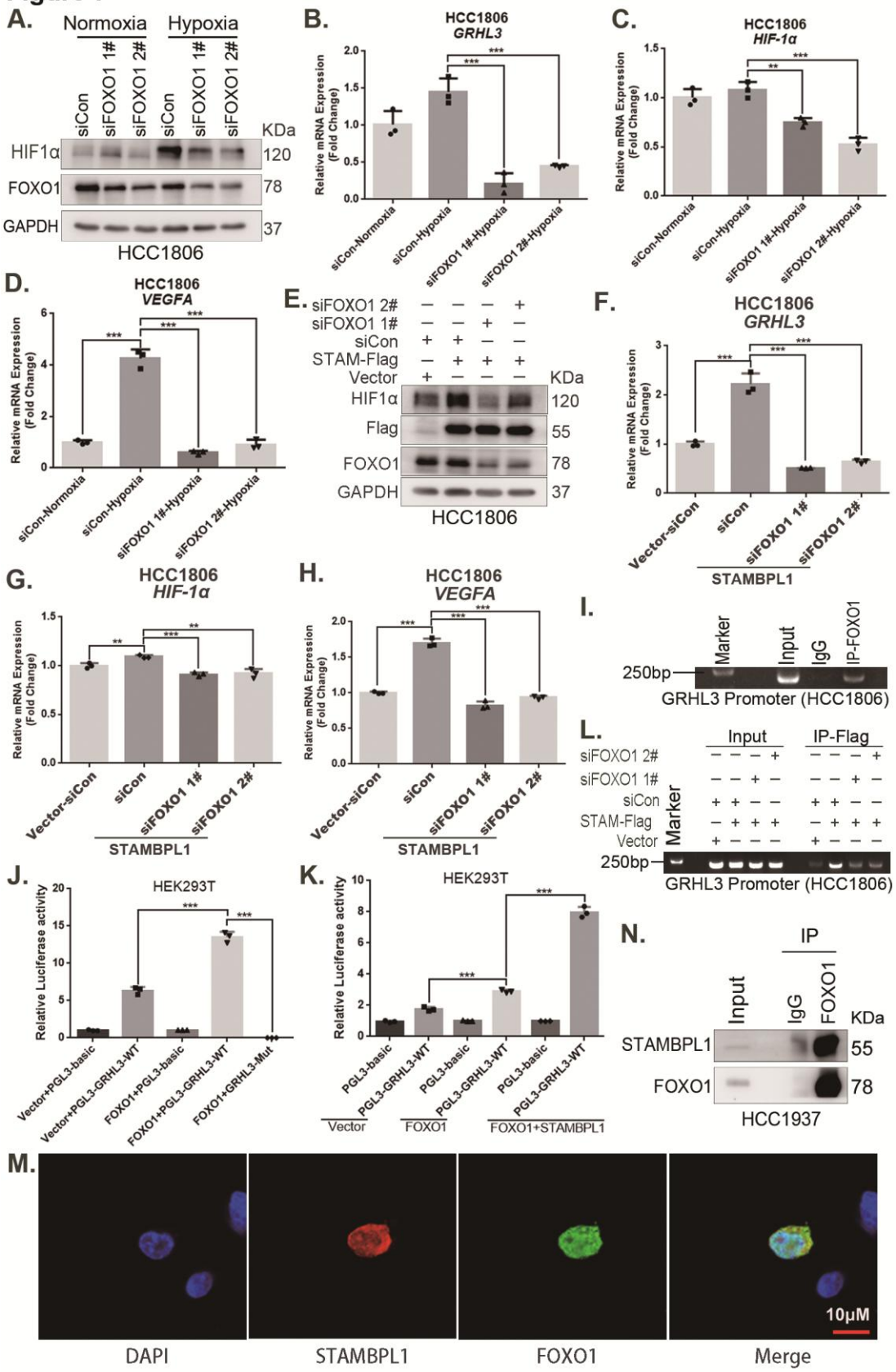
A.
Normoxia
Hypoxia
siCon
siFOXO1 1#
siFOXO1 2#
siCon
siFOXO1 1#
siFOXO1 2#
KDa
HIF1α
120
FOXO1
78
GAPDH
37
HCC1806
B.
HCC1806
GRHL3
Relative mRNA Expression (Fold Change)
siCon-Normoxia
siCon-Hypoxia
siFOXO1 1#-Hypoxia
siFOXO1 2#-Hypoxia
C.
HCC1806
HIF-1α
Relative mRNA Expression (Fold Change)
siCon-Normoxia
siCon-Hypoxia
siFOXO1 1#-Hypoxia
siFOXO1 2#-Hypoxia
D.
HCC1806
VEGFA
Relative mRNA Expression (Fold Change)
siCon-Normoxia
siCon-Hypoxia
siFOXO1 1#-Hypoxia
siFOXO1 2#-Hypoxia
E.
siFOXO1 2#
siFOXO1 1#
siCon
STAM-Flag
Vector
KDa
HIF1α
120
Flag
55
FOXO1
78
GAPDH
37
HCC1806
F.
HCC1806
GRHL3
Relative mRNA Expression (Fold Change)
Vector-siCon
siCon
siFOXO1 1#
siFOXO1 2#
STAMBPL1
G.
HCC1806
HIF-1α
Relative mRNA Expression (Fold Change)
Vector-siCon
siCon
siFOXO1 1#
siFOXO1 2#
STAMBPL1
H.
HCC1806
VEGFA
Relative mRNA Expression (Fold Change)
Vector-siCon
siCon
siFOXO1 1#
siFOXO1 2#
STAMBPL1
I.
Marker
Input
IgG
IP-FOXO1
250bp
GRHL3 Promoter (HCC1806)
L.
Input
IP-Flag
siFOXO1 2#
siFOXO1 1#
siCon
STAM-Flag
Vector
Marker
250bp
GRHL3 Promoter (HCC1806)
J.
HEK293T
Relative Luciferase activity
Vector+PGL3-basic
Vector+PGL3-GRHL3-WT
FOXO1+PGL3-basic
FOXO1+PGL3-GRHL3-WT
FOXO1+GRHL3-Mut
K.
HEK293T
Relative Luciferase activity
PGL3-basic
PGL3-GRHL3-WT
PGL3-basic
PGL3-GRHL3-WT
PGL3-basic
PGL3-GRHL3-WT
Vector
FOXO1
FOXO1+STAMBPL1
N.
IP
Input
IgG
FOXO1
KDa
STAMBPL1
55
FOXO1
78
HCC1937
M.
10μM
DAPI
STAMBPL1
FOXO1
Merge

Figure 8

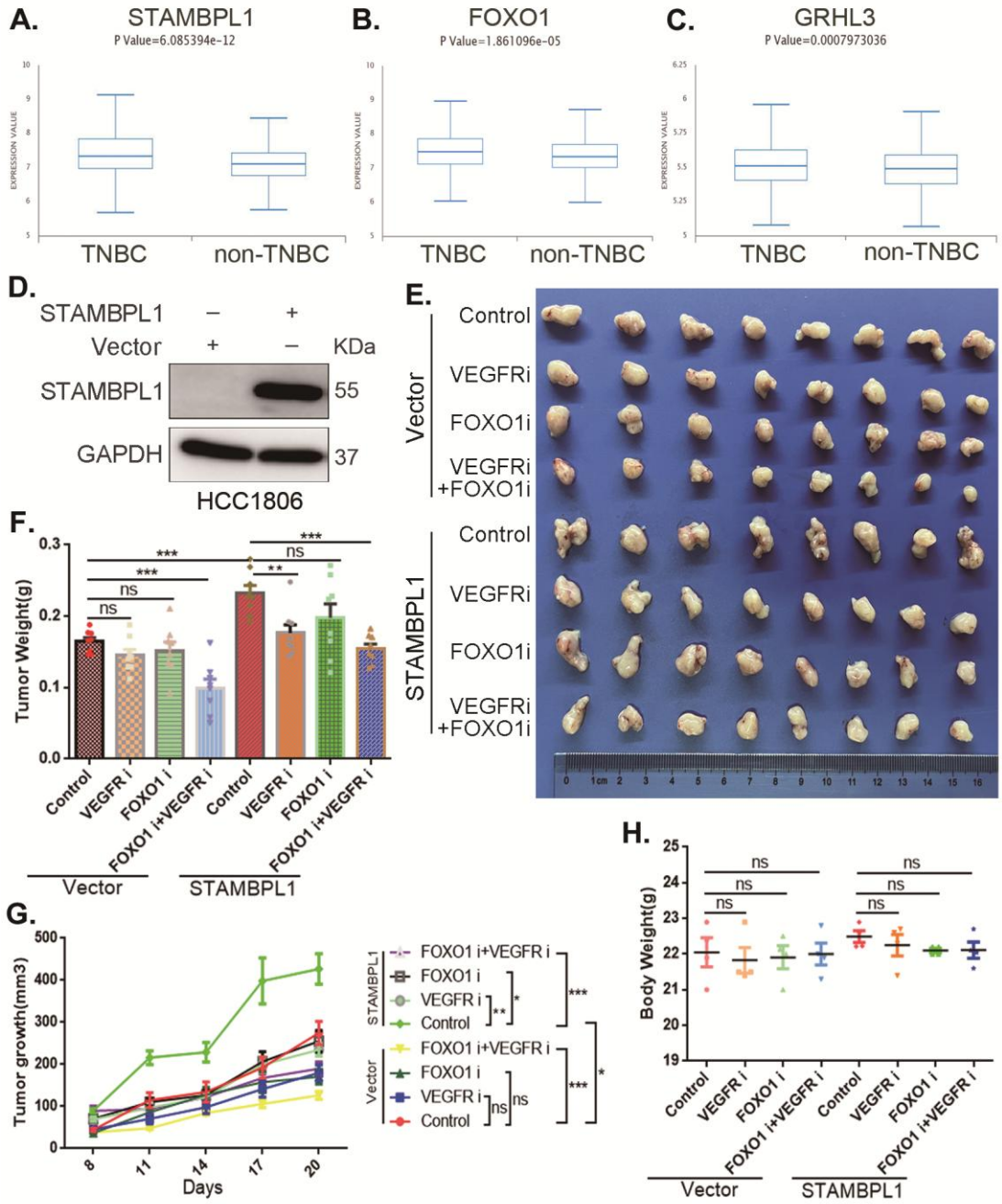
A.
STAMBPL1
P Value=6.085394e-12
EXPRESSION VALUE
TNBC
non-TNBC
B.
FOXO1
P Value=1.861096e-05
C.
GRHL3
P Value=0.0007973036
D.
STAMBPL1 – +
Vector + – KDa
STAMBPL1 55
GAPDH 37
HCC1806
E.
Vector
Control
VEGFRi
FOXO1i
VEGFRi +FOXO1i
STAMBPL1
F.
Tumor Weight(g)
Control
VEGFR i
FOXO1 i
FOXO1 i+VEGFR i
Vector
STAMBPL1
G.
Tumor growth(mm3)
Days
FOXO1 i+VEGFR i
FOXO1 i
VEGFR i
Control
H.
Body Weight(g)

Figure 9

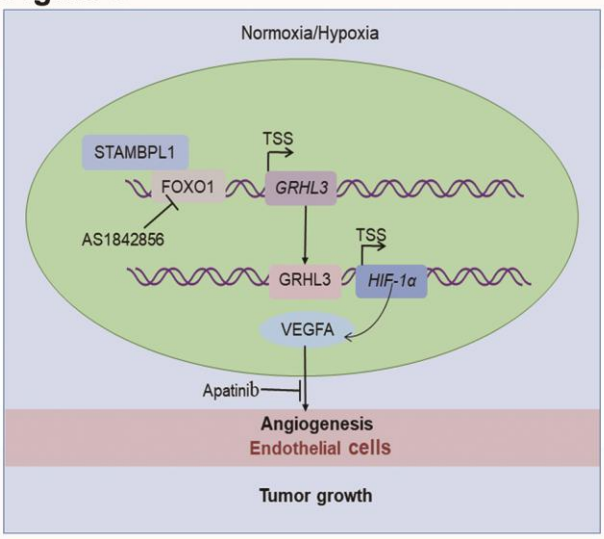
Normoxia/Hypoxia
STAMBPL1
TSS
FOXO1
GRHL3
AS1842856
TSS
GRHL3
HIF-1α
VEGFA
Apatinib
Angiogenesis
Endothelial cells
Tumor growth

Figure S1

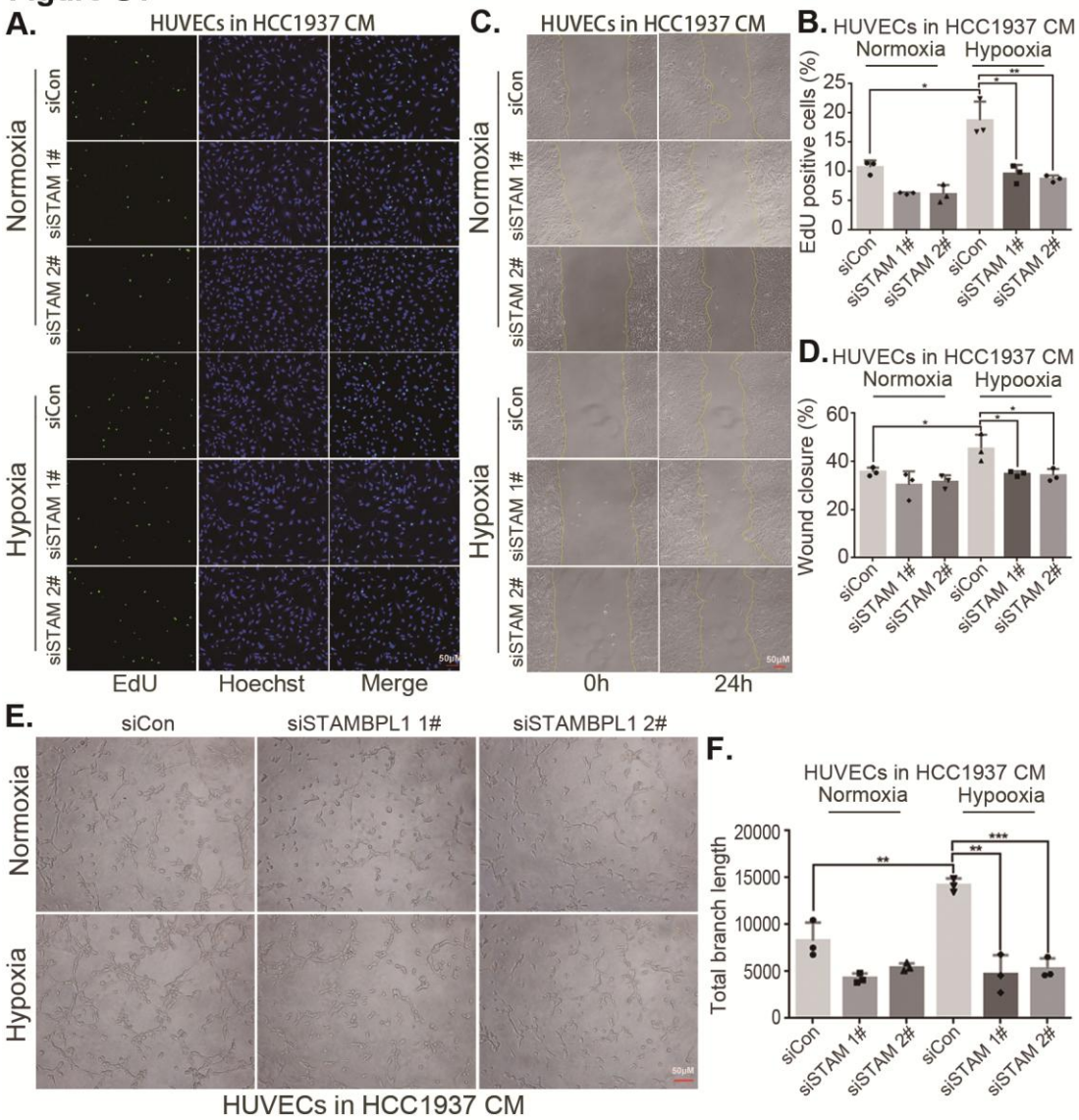
A.
HUVECs in HCC1937 CM
Normoxia
Hypoxia
siCon
siSTAM 1#
siSTAM 2#
EdU
Hoechst
Merge
C.
HUVECs in HCC1937 CM
0h
24h
B.
HUVECs in HCC1937 CM
Normoxia
Hypooxia
EdU positive cells (%)
D.
HUVECs in HCC1937 CM
Wound closure (%)
E.
siCon
siSTAMBPL1 1#
siSTAMBPL1 2#
HUVECs in HCC1937 CM
F.
HUVECs in HCC1937 CM
Total branch length

Figure S2

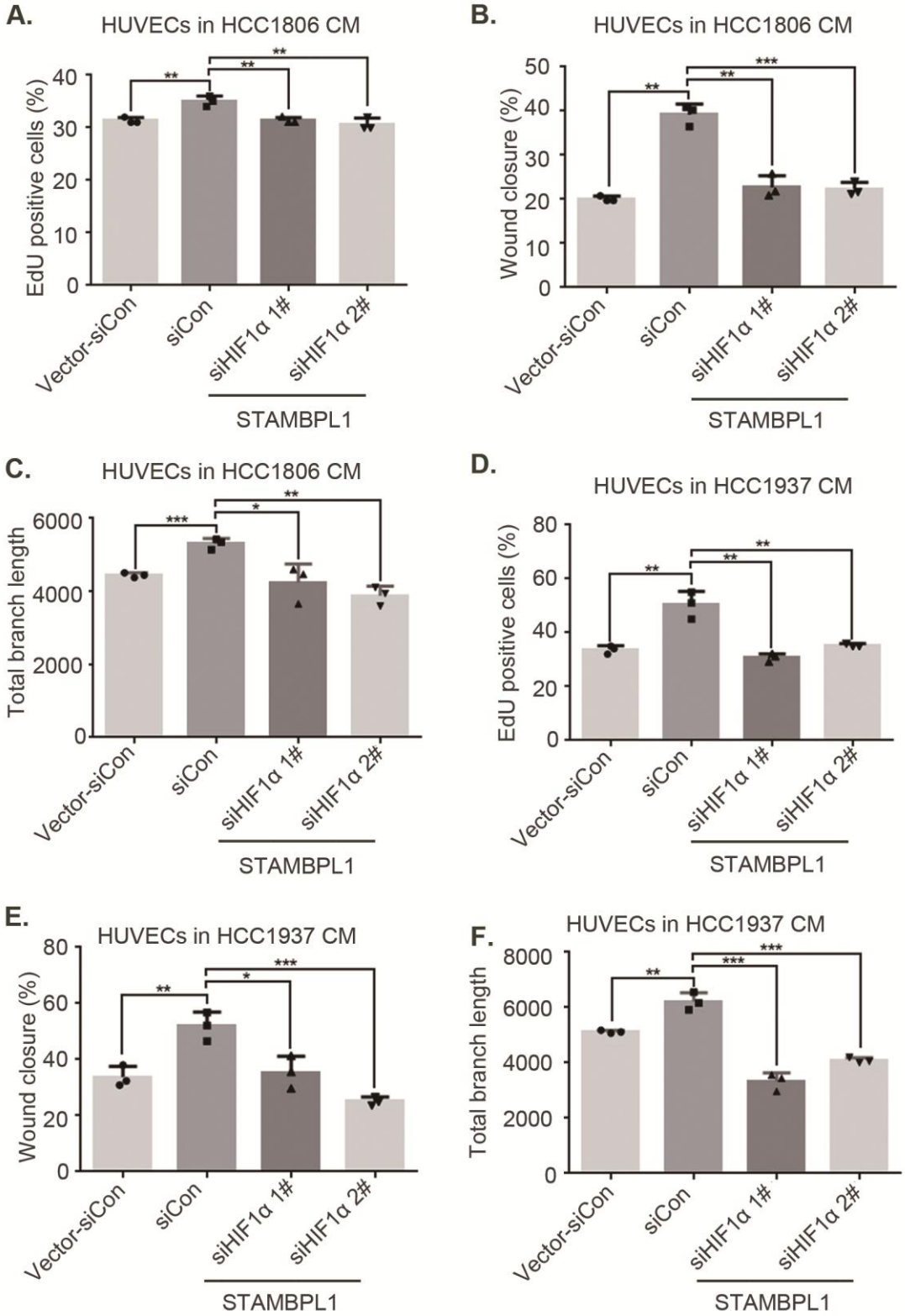
A.
HUVECs in HCC1806 CM
EdU positive cells (%)
0
10
20
30
40
**
**
**
Vector-siCon
siCon
siHIF1α 1#
siHIF1α 2#
STAMBPL1
B.
HUVECs in HCC1806 CM
Wound closure (%)
0
10
20
30
40
50
**
**
***
Vector-siCon
siCon
siHIF1α 1#
siHIF1α 2#
STAMBPL1
C.
HUVECs in HCC1806 CM
Total branch length
0
2000
4000
6000
***
*
**
Vector-siCon
siCon
siHIF1α 1#
siHIF1α 2#
STAMBPL1
D.
HUVECs in HCC1937 CM
EdU positive cells (%)
0
20
40
60
80
**
**
**
Vector-siCon
siCon
siHIF1α 1#
siHIF1α 2#
STAMBPL1
E.
HUVECs in HCC1937 CM
Wound closure (%)
0
20
40
60
80
**
*
***
Vector-siCon
siCon
siHIF1α 1#
siHIF1α 2#
STAMBPL1
F.
HUVECs in HCC1937 CM
Total branch length
0
2000
4000
6000
8000
**
***
***
Vector-siCon
siCon
siHIF1α 1#
siHIF1α 2#
STAMBPL1

Figure S3

A.

Gene name	siSTAM#1	*P* value	siSTAM#2	*P* value
VWA5B1	-1.796	0.018	-2.357	0.005
TMX2-CTNND1	-1.743	0.038	-1.998	0.007
SLFN12L	-1.676	0.039	-1.840	0.026
CSF1R	-1.655	0.020	-1.585	0.027
NCF2	-1.649	0.000	-1.571	0.000
RPS17	-1.600	0.001	-1.028	0.034
PRTG	-1.577	0.030	-1.708	0.031
GRHL3	-1.567	0.000	-1.068	0.007
CYP4F3	-1.482	0.001	-1.080	0.013
RARB	-1.350	0.001	-1.534	0.001
DDC8	-1.328	0.036	-1.504	0.045
GNE	-1.239	0.000	-1.134	0.017
CSF2RA	-1.198	0.017	-2.169	0.005
CP	-1.158	0.000	-1.326	0.000
SHH	-1.152	0.004	-1.300	0.002
MUC16	-1.120	0.000	-1.673	0.000
MFAP3L	-1.053	0.013	-1.278	0.004
DAPK1	-1.030	0.000	-1.367	0.000

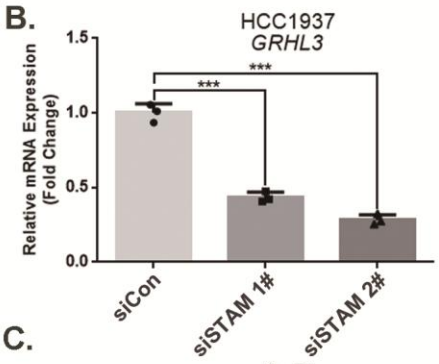

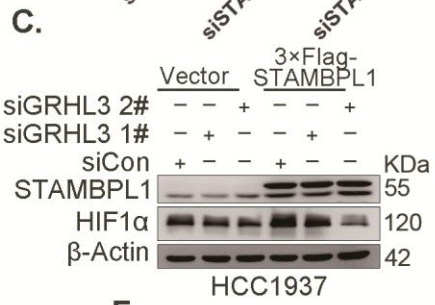

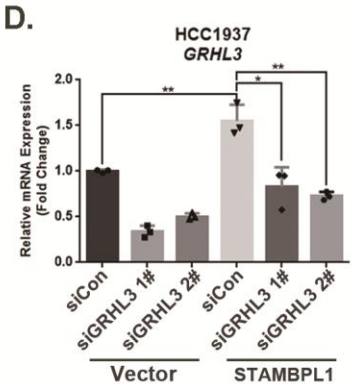

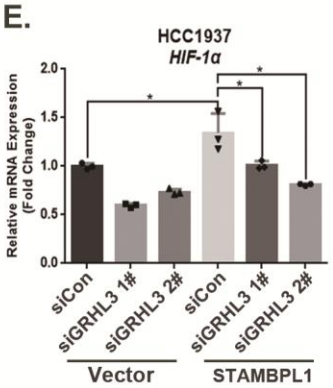

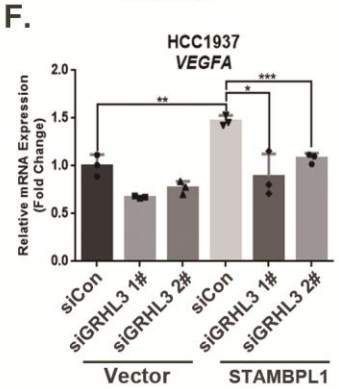

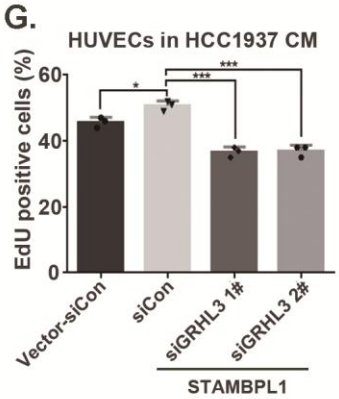

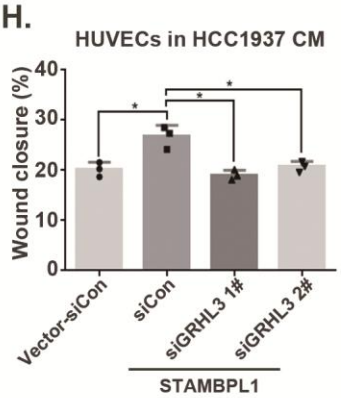

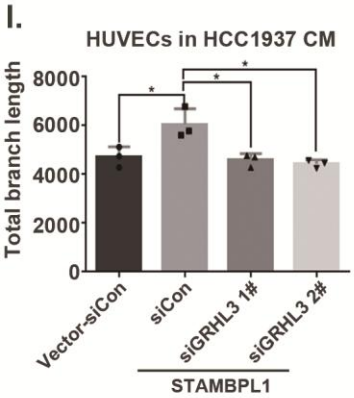

Figure S4

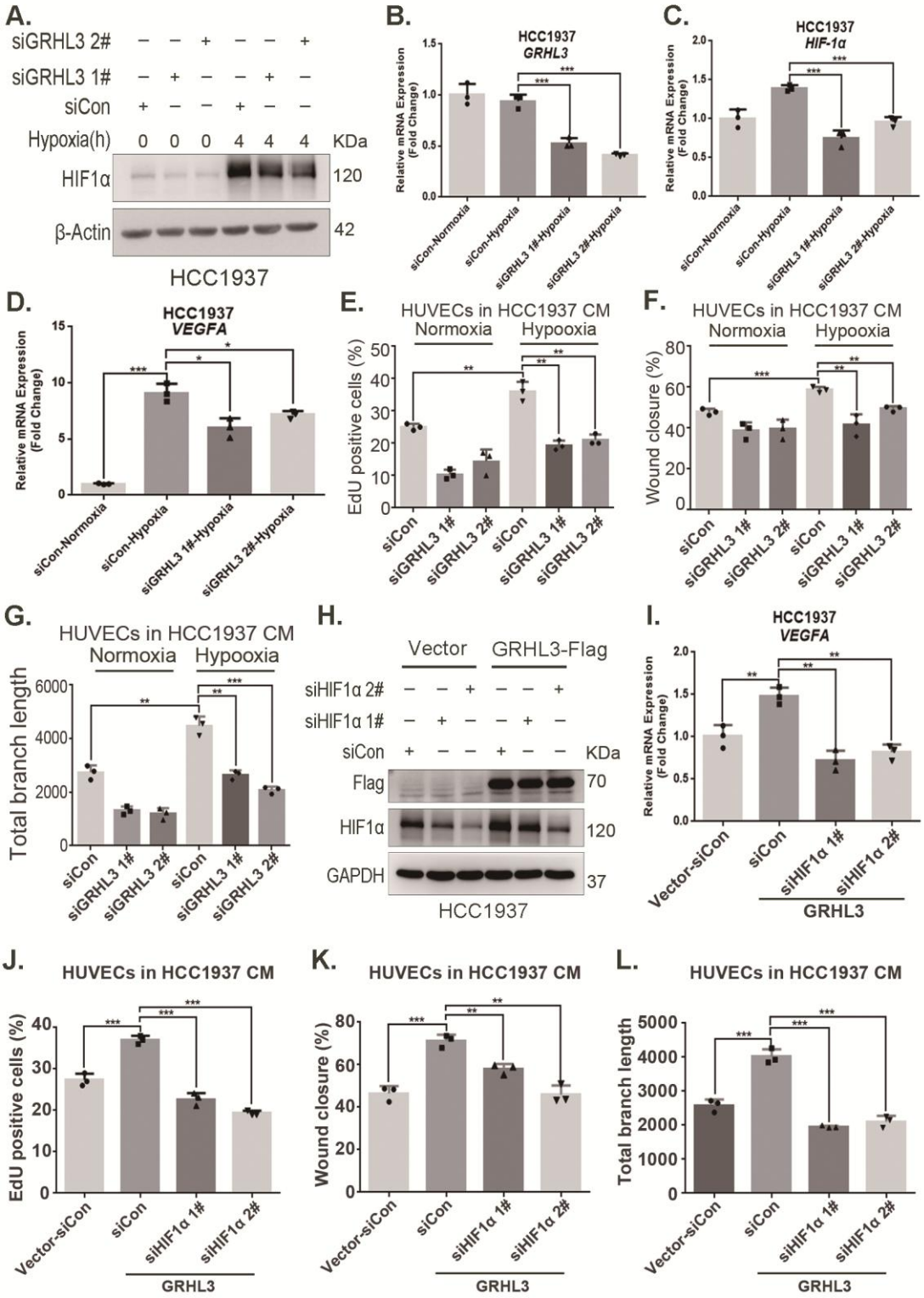
A.
siGRHL3 2#
siGRHL3 1#
siCon
Hypoxia(h) 0 0 0 4 4 4 KDa
HIF1α 120
β-Actin 42
HCC1937
B.
HCC1937
GRHL3
Relative mRNA Expression (Fold Change)
siCon-Normoxia
siCon-Hypoxia
siGRHL3 1#-Hypoxia
siGRHL3 2#-Hypoxia
C.
HCC1937
HIF-1α
D.
HCC1937
VEGFA
E.
HUVECs in HCC1937 CM
Normoxia
Hypooxia
EdU positive cells (%)
siCon
siGRHL3 1#
siGRHL3 2#
F.
Wound closure (%)
G.
Total branch length
H.
Vector
GRHL3-Flag
siHIF1α 2#
siHIF1α 1#
siCon
KDa
Flag 70
HIF1α 120
GAPDH 37
HCC1937
I.
Vector-siCon
siHIF1α 1#
siHIF1α 2#
GRHL3
J.
HUVECs in HCC1937 CM
K.
L.

Figure S5

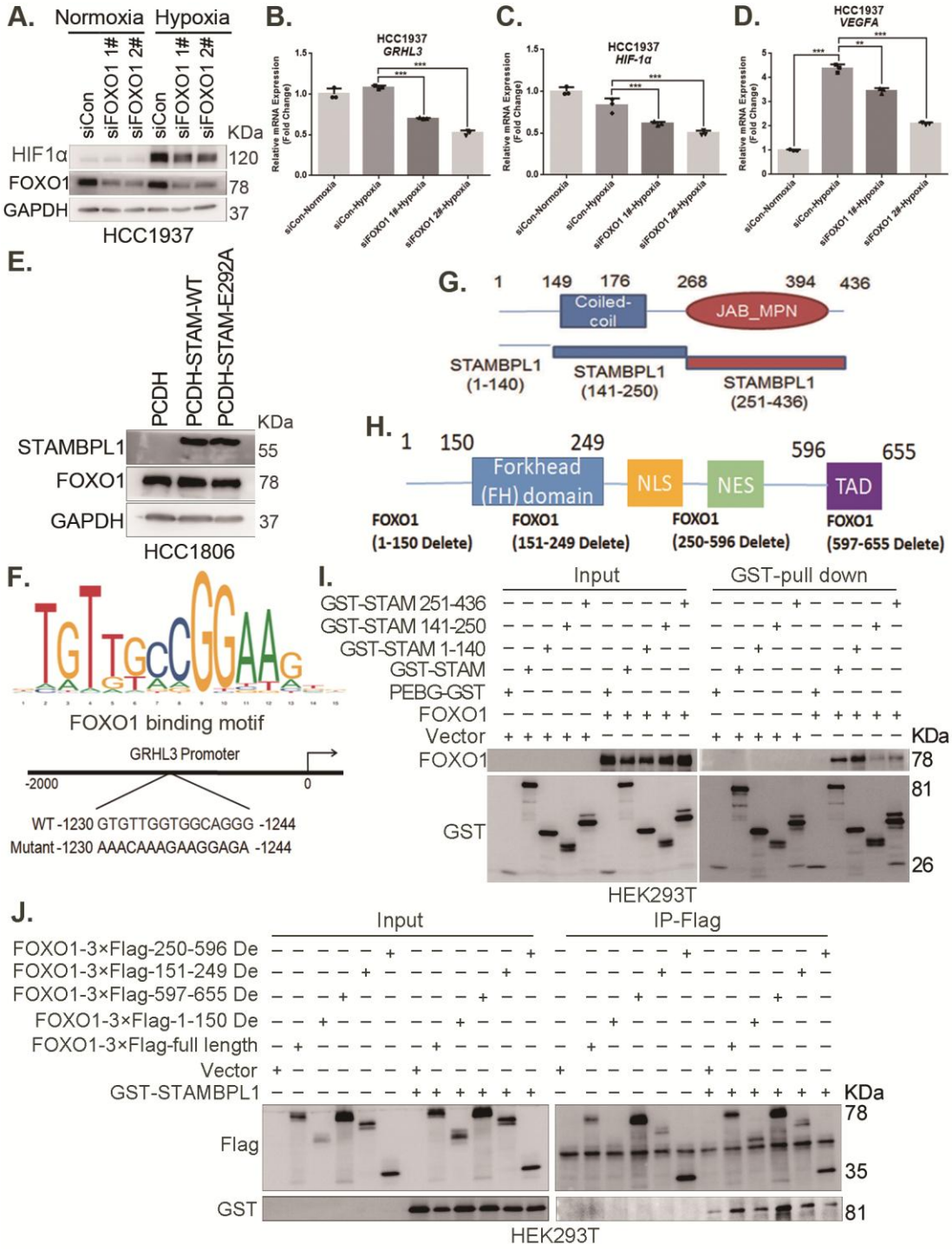
A.
Normoxia
Hypoxia
siCon
siFOXO1 1#
siFOXO1 2#
siCon
siFOXO1 1#
siFOXO1 2#
KDa
HIF1α
FOXO1
GAPDH
120
78
37
HCC1937
B.
HCC1937
GRHL3
Relative mRNA Expression (Fold Change)
siCon-Normoxia
siCon-Hypoxia
siFOXO1 1#-Hypoxia
siFOXO1 2#-Hypoxia
C.
HCC1937
HIF-1α
D.
HCC1937
VEGFA
E.
PCDH
PCDH-STAM-WT
PCDH-STAM-E292A
KDa
STAMBPL1
FOXO1
GAPDH
55
78
37
HCC1806
G.
1
149
176
268
394
436
Coiled-coil
JAB_MPN
STAMBPL1 (1-140)
STAMBPL1 (141-250)
STAMBPL1 (251-436)
H.
1
150
249
596
655
Forkhead (FH) domain
NLS
NES
TAD
FOXO1 (1-150 Delete)
FOXO1 (151-249 Delete)
FOXO1 (250-596 Delete)
FOXO1 (597-655 Delete)
F.
FOXO1 binding motif
GRHL3 Promoter
-2000
0
WT -1230 GTGTTGGTGGCAGGG -1244
Mutant -1230 AAACAAAGAAGGAGA -1244
I.
Input
GST-pull down
GST-STAM 251-436
GST-STAM 141-250
GST-STAM 1-140
GST-STAM
PEBG-GST
FOXO1
Vector
KDa
FOXO1
GST
78
81
26
HEK293T
J.
Input
IP-Flag
FOXO1-3×Flag-250-596 De
FOXO1-3×Flag-151-249 De
FOXO1-3×Flag-597-655 De
FOXO1-3×Flag-1-150 De
FOXO1-3×Flag-full length
Vector
GST-STAMBPL1
KDa
Flag
GST
78
35
81
HEK293T

Figure S6

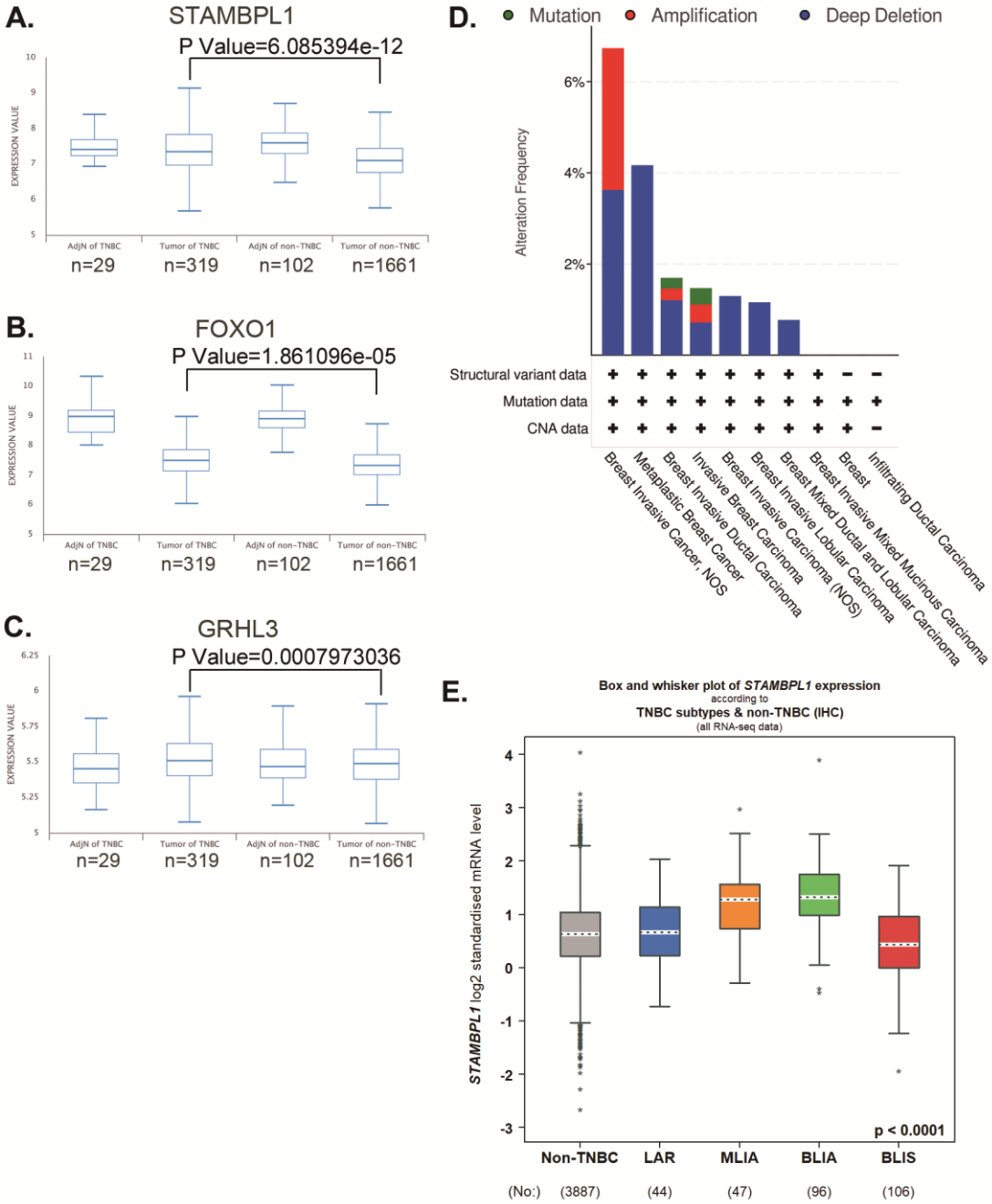
A.
STAMBPL1
P Value=6.085394e-12
EXPRESSION VALUE
AdjN of TNBC
Tumor of TNBC
AdjN of non-TNBC
Tumor of non-TNBC
n=29
n=319
n=102
n=1661
B.
FOXO1
P Value=1.861096e-05
EXPRESSION VALUE
AdjN of TNBC
Tumor of TNBC
AdjN of non-TNBC
Tumor of non-TNBC
n=29
n=319
n=102
n=1661
C.
GRHL3
P Value=0.0007973036
EXPRESSION VALUE
AdjN of TNBC
Tumor of TNBC
AdjN of non-TNBC
Tumor of non-TNBC
n=29
n=319
n=102
n=1661
D.
Mutation
Amplification
Deep Deletion
Alteration Frequency
6%
4%
2%
Structural variant data
Mutation data
CNA data
Breast Invasive Cancer, NOS
Metaplastic Breast Cancer
Breast Invasive Ductal Carcinoma
Invasive Breast Carcinoma
Breast Invasive Carcinoma (NOS)
Breast Invasive Lobular Carcinoma
Breast Mixed Ductal and Lobular Carcinoma
Breast Invasive Mixed Mucinous Carcinoma
Breast Infiltrating Ductal Carcinoma
E.
Box and whisker plot of STAMBPL1 expression
according to
TNBC subtypes & non-TNBC (IHC)
(all RNA-seq data)
STAMBPL1 log2 standardised mRNA level
p < 0.0001
Non-TNBC
LAR
MLIA
BLIA
BLIS
(No:)
(3887)
(44)
(47)
(96)
(106)